2021

Development of Endoplasmic Reticulum Targeted Probes and Red Fluorescent Probes for Detecting Zinc

Drew Maslar

Development of endoplasmic reticulum targeted probes and red fluorescent probes for detecting zinc

_____

A Thesis

Presented to

the Faculty of the College of Natural Sciences and Mathematics

University of Denver

_____

In Partial Fulfillment

of the Requirements for the Degree

Master of Science

_____

by

Drew Maslar

June 2021

Advisor: Yan Qin

Author: Drew Maslar
Title: Development of endoplasmic reticulum targeted probes and red fluorescent probes for detecting zinc
Advisor: Yan Qin
Degree Date: June 2021

Abstract

Zinc (Zn^{2+}) is the second most abundant transition metal in the body and is important in various biological functions. Fluorescent sensors based on circularly permuted fluorescent proteins (cpFPs) have been previously made to detect labile, or unbound, Zn^{2+} within the cytoplasm of cells. These sensors have proven invaluable for studying Zn^{2+}, however, these sensors are limited to their use in the cytoplasm and by the fact that only green cpFP have been utilized to create fluorescent Zn^{2+} sensors. In this thesis, we use a combination of peptide targeting sequences, site-directed mutagenesis, and rational design to target the currently developed cpFP Zn^{2+} sensors to the lumen of the endoplasmic reticulum (ER), and expand the tool kit of cpFP Zn^{2+} sensors by introducing the first generation of red-shifted cpFP Zn^{2+} sensors. We demonstrate that not only can these Zn^{2+} sensors be targeted to the ER, but they can functionally be used to estimate labile ER Zn^{2+} concentration. We also show that red-shifted cpFP Zn^{2+} sensors display high sensitivity for detecting labile Zn^{2+}, similar to the green-shifted cpFP Zn^{2+} sensors. These discoveries add to the current knowledge of labile Zn^{2+} within the lumen of the ER and introduce a new sensor that allows for the observation of labile Zn^{2+} in cells that was previously unavailable.

Table of Contents

List of Figures

3.0

4.0

1.0 INTRODUCTION

1.1 Zinc biology

Zn^{2+}, being the second most abundant transition metal in the body, has been identified as a crucial transition metal within mammalian cells. In fact, it is estimated that Zn^{2+} interacts with ~10% of the human proteome, which is ~2800 proteins (Andreini et al. 2006). Because of this, understanding Zn^{2+} homeostasis is critical for helping treat a variety of diseases and conditions. Studies that implicate Zn^{2+} as an important transition metal range from focusing on neurodegeneration, diabetes, and apoptosis, to mental diseases and more, reviewed here (Chasapis et al. 2020). Recently, it has been shown that Zn^{2+} can be shuttled from the lysosome to the cytoplasm through a channel protein known as TRMPL1, and dysfunction of this protein is a genetic cause of Mucolipidosis Type IV, a disease characterized by severe neurodegeneration and neurological underdevelopment (Minckley et al. 2019). Elucidation of labile Zn^{2+} flux, concentration, and biological functions require fluorescent probes that can detect changes in cellular Zn^{2+} concentrations.

1.2 Zinc sensors

An invaluable tool that helped elucidate Zn^{2+}'s importance in biology is fluorescent Zn^{2+} sensors. The principal behind fluorescent Zn^{2+} sensors is that their fluorescent spectra are dependent on the concentration of labile Zn^{2+}. For example, the

turn-on fluorescent Zn^{2+} sensors will increase in fluorescence when excited at a specific wavelength if labile Zn^{2+} concentration increases and decrease in fluorescence if labile Zn^{2+} concentration decreases. Fluorescent Zn^{2+} sensors are typically characterized by their affinity (K_d) for Zn^{2+}, their kinetics (the time it takes to go from maximal to minimal fluorescence), their dynamic range (F_{max}/F_{min}) from an apo- to saturated states), and their specificity for Zn^{2+}. In addition to this, Zn^{2+} sensors are studied in the presence of other cellular cations, such as Mg^{2+} and Ca^{2+}, and various pH's to identify if there is any fluorescent change of the sensors that are independent of Zn^{2+}. Ideally, a good Zn^{2+} sensor has a K_d that is around biological relevant concentrations of Zn^{2+}, a high dynamic range, is exclusively specific for Zn^{2+}, and is largely unaffected by changes in pH. Current Zn^{2+} sensors include both small molecule sensors and genetically encoded sensors.

1.3 Small molecule Zn^{2+} sensors

Historically, it was found that Zn^{2+} produces fluorescence in solution with the small molecule 8-quinolinol (Mahanand and Houck 1968). However, this sensor was found to be heavily affected by pH and fluoresce in the presence of Mg^{2+} and Ca^{2+}. Improvements of small molecule Zn^{2+} sensors were sought to help facilitate the study of Zn^{2+}. About 30 years after the discovery of 8-quinolinol, the Zinpyr family of small molecule Zn^{2+} sensors was made (Burdette et al. 2001). Zinpyr-1 and -2 show a 3-5 fold dynamic range and are highly specific for Zn^{2+} and show no fluorescent change upon addition of 5mM Mg^{2+} or Ca^{2+}. However, Zinpyrs are still largely affected by pH changes.

Creation of the FluoZin family of small molecule sensors not only largely solved the issue of pH dependent fluorescent changes, but also introduced small molecule Zn^{2+} sensors that show up to a 200-fold increase in fluorescence upon the introduction of Zn^{2+} (Gee et al. 2002). Although these sensors do respond to Ca^{2+}, the concentration of Ca^{2+} needed to illicit a response is above physiological Ca^{2+} levels, (Ca^{2+} > 5mM.

Overall, small molecule Zn^{2+} sensors have become convenient tools for studying Zn^{2+}. They are cell permeable, have high dynamic ranges, fast kinetics, and offer a large selection of small molecule sensors to select from (Dean, Qin and Palmer 2012).

Small molecule Zn^{2+} sensors, however, are not available without caveats. Although the FluoZin family of Zn^{2+} sensors are largely pH insensitive and show a high dynamic range, this family of Zn^{2+} sensors has a K_d for Zn^{2+} of 15nM (FluoZin-3) to 7.8μM (FluoZin-1), reaching out of the biologically relevant concentration of labile Zn2+.

Beyond some small molecule Zn^{2+} sensors having low affinity for Zn^{2+}, small molecules are not efficiently targeted to any organelle in the cell. Colocalization analysis have been done to identify intracellular compartments that contain small molecule Zn^{2+} sensors (Rivera-Fuentes et al. 2015), and powerful small molecule sensors such as FluoZin-3 seem to localized to additional cellular compartments in addition to the cytoplasm (Qin et al. 2013), but this may be due to the sequestering of small molecules to a cellular compartment and independent of labile Zn^{2+} concentrations. The FluoZin sensors have also been shown to change physiological levels of Zn^{2+} (Krezel and Maret 2006), which can result in inaccurate measurements of labile Zn^{2+}. Due to their cell

permeability, small molecule Zn^{2+} sensors are not typically good for long-term imaging as they can leak out of the cell.

1.4 Genetically encoded FRET Zn^{2+} sensors

Genetically encoded Zn^{2+} sensors refer to Zn^{2+} sensors that are encoded by DNA. These sensors pose an advantage for studying Zn^{2+} because they allow for the expression of these sensors in 2D-cell cultures and transgenic organisms, but also allows for the efficient targeting of these sensors to specific cellular compartments through peptide targeting sequences. These sensors have also been shown to not perturb physiological Zn^{2+} (Qin et al. 2013).

The first iteration of genetically encoded Zn^{2+} sensors came in the form of FRET (Förster resonance energy transfer) sensors. FRET sensors use Zn^{2+} binding motifs to either increase or decrease FRET ratio in the presence of labile Zn^{2+}. One of the first generations of FRET Zn^{2+} sensors were the CALWY sensors (van Dongen et al. 2006). This sensor, using a copper chaperone protein, Atox1, fused to CFP and WD4 fused to YFP, was originally trying to develop a sensor for copper, but unexpectedly found that this sensor had a K_d for Zn^{2+} of ~350pM.

The unexpected development of the FRET Zn^{2+} sensors led to an interest in further improving these sensors. The first improvement of these sensors was focused on fusing ATOX1-CFP and WD4-YFP through a flexible linker of varying peptide lengths, and identifying the properties of the sensors (van Dongen et al. 2007). It was found that the length of the flexible linker does affect affinity for Zn^{2+} and dynamic range. In fact, the

CALWY sensor with the longest linker region, named CA-L9-WY, showed a 170fM K_d for Zn^{2+} and a FRET ratio change of ~0.9 fold, whereas CA-L2-WY with the shortest linker region showed a 1.4pM K_d and a FRET ratio change of ~1.4 fold.

eCALWY sensors were generated from the original CALWY sensors by using a cerulean and citrine FRET pair as oppose to CFP and YFP (Vinkenborg et al. 2009). Again, both affinity for Zn^{2+} and dynamic range were altered by this simple change. Beyond exploring different FRET pairs to use in Zn^{2+} sensors, the original work with eCALWYs included mutated cysteines involved in Zn^{2+} binding to reduce the affinity of the sensor to Zn^{2+}. This work also attempted to fuse the sensors to VAMP2 to achieve localization to secretory granules. Although the localization was efficient, eCALWYs did not work in these vesicles.

The next generation of Zn^{2+} FRET sensors was the Zif268 sensors. This sensor used the Zif268 binding domain to bring CFP and YFP together in the presence of Zn^{2+} (Dittmer et al. 2009). Due to the known Zn^{2+} coordination sites of Zif268, which are two cysteines and two histidines (Cys_2His_2), mutant sensors of varying affinities were able to be easily made. The WT Zif268 sensor showed an ~2.2 fold increase in FRET ratio and has a K_d of 1.6μM, whereas a mutant sensor where both cysteines were mutated to histidines (Cys_2His_2 to His_4), showed a 4-fold FRET ratio increase and has a 160μM affinity for Zn^{2+}. These sensors were also functional after successfully targeting to the mitochondria and plasma membrane.

Following the creation of Zif268 FRET Zn^{2+} sensors, a new FRET Zn^{2+} sensor using zinc finger 1 and 2 (ZF1, ZF2) from the yeast protein Zap1 was used to increase

FRET of eCFP and eYFP (Qiao et al. 2006, Qin et al. 2011). With new Zn^{2+} binding proteins, the FRET ratio of this sensor showed only an ~1.3 fold increase in FRET ratio in the presence of Zn^{2+}. Because the FRET ratio showed no improvement over previous FRET Zn^{2+} sensors, the eCFP was truncated and the eYFP was replaced with citrine, mutations were made in Zn^{2+} binding domains of the ZFs and, importantly, mutations in the linker regions between the FPs and ZFs were made. The resulting sensors, named ZapCY1 and ZapCY2 showed a 4.15 fold and 1.4 fold dynamic range, respectively, and an affinity of 2.5pM and 811pM, respectively. ZapCY1 and ZapCY2 were used to study labile Zn^{2+} concentration of the endoplasmic reticulum (ER) and Golgi apparatus. Both compartments were estimated to have a low liable Zn^{2+} concentration, 0.9pM for the ER and 0.6pM for the Golgi.

The versatility of FRET Zn^{2+} sensors was shown when the Zap FRET sensors were used as a platform to create multiple sensors with different FRET pairs (Miranda et al. 2012). Seven different FRET sensors were made with excitation spectrum ranging from 435 to 486nm and emission spectrum from 535nm to 605nm. The advantage of having a wide pallet of genetically encoded sensors is that multiplex imaging is possible with a combination of two sensors localized to different parts of the cell with different excitation spectra. Miranda et al. imaged Zn^{2+} simultaneously in multiple compartments such as the ER, Golgi, and mitochondria.

FRET sensors are a useful tool for studying Zn^{2+}. They introduced the ability to measure and observe labile Zn^{2+} in specific cellular compartments as well as allow for multiplex imaging. An array of affinities for Zn^{2+} are also found across the many sensors

that were developed. Genetically encoded FRET sensors, however, did not overcome all caveats of Zn^{2+} sensors. FRET sensors have slower kinetics compared to small molecule sensors as they depend on protein conformational changes to produce differences in FRET, and like most FPs, FRET sensors are prone to changes in fluorescence due to changes in pH. They also have relatively low dynamic ranges compared to small molecule sensors.

1.5 Genetically encoded single FP Zn^{2+} sensors

In order to create a sensor that can confer both the genetic encodability and high sensitivity, single fluorescent protein-based Zn^{2+} sensors were developed. Commonly, these sensors utilize a cpFP and fuse ZF2 and ZF1 to the new N- and C-terminus, respectively. Originally this design for cation sensors was used for the Ca^{2+} sensors known as pericams (Nagai et al. 2001). The N- and C-terminus of the cpFPs are found in the β-barrel of the FP, this causes the chromophore to be exposed to solvents and reduces the fluorescence of the FP. By inserting, in the case of Zn^{2+} sensors, Zn^{2+} binding domains on each terminus, in the presence of Zn^{2+}, the binding domains will form a complex and block the chromophore from solvents, therefore increasing the brightness of the FP; this allows for the correlation of brightness to labile Zn^{2+} concentration. Single FP genetically encoded Zn^{2+} sensors have been shown to also have a range of affinities for Zn^{2+}, have faster kinetics, and display much larger dynamic ranges compared with FRET Zn^{2+} sensors.

The GZnP family of Zn^{2+} sensors were introduced. The GZnP family of sensors were made using the same model as the G-CaMP3 Ca^{2+} sensors (Tian et al. 2009), which utilized a cpEGFP with calmodulin fused to the C-terminus through a linker region and a

M13 calmodulin binding peptide fused to the N-terminus, also through a linker region; GZnP used ZF2 and ZF1, fused to the N- and C-terminus respectively, instead of the calcium binding domains (Qin et al. 2016). GZnP1 was developed mostly through mutations within the linker regions between the ZFs and cpGFP, named linker 1 and linker 2 for the linkers fused to ZF1 and ZF2, respectively, the Zn^{2+} binding domains in ZF1 and ZF2, and mutations in the cpEGFP FP.

GZnP1 exhibited a dynamic range of 2.2 fold and a K_d of 34pM. Although the dynamic range of GZnP1 is still no significant improvement over the FRET sensors or GEZI sensors, the kinetics were on the order of seconds for the sensor to turn-off and on and GZnP1 was able to be efficiently targeted to the mitochondria and plasma membrane.

Following the creation of GZnP1, two years later, GZnP2 was added to the GZnP family. GZnP2 was created through bacterial screening methods focusing on mutations within the linker 1 and 2 regions of GZnP1 (Fudge et al. 2018), which is a strategy that has been employed in the past with improving Ca^{2+} sensors (Akerboom et al. 2012). Specifically, a mutation of linker 2 from THLE to PHLE is what created GZnP2. GZnP2 showed the same kinetic and localization abilities as GZnP1, but importantly showed an improved dynamic range of ~4.5 fold. The affinity for Zn^{2+} was lower in GZnP2, 352pM, compared to GZnP1.

The newest addition to the GZnP family of sensors is GZnP3, that once again, was made from mutating linker 2 of GZnP2 to ILLE (Minckley et al. 2019). GZnP3 showed the highest dynamic range of all sensors with an ~10 fold increase in fluorescence. GZnp3 is also the lowest affinity sensor for Zn^{2+} with a K_d of 1.3nM. Compared to GZnP1 and

GZnP2, GZnP3 is dim at resting conditions in cells. However, due to its high dynamic range, the sensor yields a high sensitive response to changes in cellular Zn^{2+}, allowing GZnP3 to reveal the first discovery that Zn^{2+} can be released from intracellular vesicles to the cytosol.

Another type of singe FP based genetically encoded fluorescent Zn^{2+} indicator (GEZIs) were developed in Dr. Huiwang Ai lab. Three GEZIs were designed, two using a monomeric teal fluorescent protein (mTFP1), and one using mApple. ZnGreen1 and ZnRed did not utilize a cpFP, but instead inserted truncated Zap1 protein (Zap1 1-65) into the β-barrel of mTFP1; ZnGreen2 followed the cpFP model of pericams and other Ca^{2+} sensors (Chen and Ai 2016). ZnGreen1 showed a K_d of 633nM and ZnGreen2 a K_d of 20μM, ZnRed showed two binding affinities of 166nM and 20μM.

Both ZnGreen1 and 2 are turn-off Zn^{2+} sensors, as in instead of an increase in fluorescence in the presence of labile Zn^{2+}, the fluorescence decreases. In HEK293T cells, ZnGreen1 showed ~3.33 fold decrease in fluorescence upon the addition of Zn^{2+}, however, it took almost 10min for the fluorescence to reach a minimum. Because the movement of Zn^{2+} intracellularly can happen in less than a second (Minckley et al. 2019), sensor kinetics that are this slow may not resolve important biological information of transient Zn^{2+} flux, and therefore, are not ideal. ZnRed is a turn-on sensor that has an improved dynamic range of ~6.5, considerably higher than previous FRET sensors, but shows the same slow kinetic properties of ZnGreen1.

Genetically encoded Zn^{2+} sensors, specifically within the GZnP family, have been successfully targeted to subcellular targets using peptide targeting sequences or through

fusion to proteins that have specific subcellular localizations. Beginning with GZnP1, this sensor was successfully targeted to the plasma membrane and mitochondria through their respective peptide targeting motifs (Qin et al. 2016). It was reported that localizing the single FP sensors to the plasma membrane and mitochondria resulted in a slight, ~2.5 fold to ~2.2 fold, reduction in dynamic range; however, this reduction is less than the reduction of dynamic range seen in localization of FRET sensors.

When GZnP2 was developed, it was not only targeted to the mitochondrial matrix through a mitochondrial localization peptide, but the mitochondrial intermembrane space through fusing GZnP2 to the second mitochondria derived activator of caspases (SMAC) (Fudge et al. 2018). Importantly, this localization was done in multiple cell types (Cos-7, HeLa, HEK293, and INS-1). Utilizing GZnP2 in different mitochondrial compartments, it was found that the intermembrane space of the mitochondria contains similar Zn^{2+} concentrations as the cytoplasm. Interestingly, the mitochondrial matrix contains almost no labile zinc in all cells tested expected for HEK293 cells.

Finally, GZnP3 was used in lysosomal related studies, and because of this, by fusing GZnP3 to proteins, targeted to the cytoplasmic facing membrane of lysosomes through TRPML1 or LAMP1, late endosomes through TRPML1 or Rab7a, and synaptic vesicles through TRPML1 and VAMP2. All fusion proteins, except LAMP1-GZnP3, functioned similarly to cytoplasmic GZnP3; LAMP1-GZnP3 showed a greatly reduced dynamic range compared to the other fusion proteins.

1.6 Single FP red Zn^{2+} sensors

Despite the success of green single FP Zn^{2+} sensors developments, functional red-shifted single FP Zn^{2+} sensors are currently unavailable. The only published red single FP Zn^{2+} sensor is called ZnRed, which has very slow kinetics and can be biologically irrelevant (Chen and Ai 2016).

In the past few years, our lab has developed several prototype red Zn^{2+} sensors, RZnPs, based off the similar platform used in the GZnP family. However, these prototype sensors suffer from either small dynamic range or unstable maximal fluorescence.

1.7 Thesis specific aims

The goal of this thesis is to develop the first generation of RZnP sensors using either RZnP0.41 or RZnP0.81 as parent sensors. Currently, the field of Zn^{2+} lacks a biologically relevant red fluorescent zinc sensor. With a red fluorescent Zn^{2+} sensors, we would be able to measure Zn^{2+} concentration in two cellular compartments simultaneously, the excitation light to detect the sensor is less toxic to cells, allowing for long term imaging experiments, and red FPs are typically more pH resistant than green FPs (Botman et al. 2019). Specifically, we are trying to achieve a RZnP that has a dynamic range of at least 2.5 fold, has kinetics similar to our GZnPs, has a stable response to TPEN and Zn^{2+}, and has modest baseline fluorescence.

Also, for the first time, we localize GZnP1 and GZnP3 to the ER through two different methods of localization. We achieve luminal ER expression of our GZnPs through the fusion of a signal sequence (SS) and KDEL, and through a transmembrane protein with a

cytoplasmic KKYN motif to achieve ER localization. This was done to address the debate of labile concentration of Zn^{2+} within the ER of HeLa cells. Currently, published estimates of labile ER Zn^{2+} concentrations include ~0.9pM (Qin et al. 2011) and >5nM (Chabosseau et al. 2014). These estimations were both made using FRET Zn^{2+} sensors. There have been no estimations made with a single FP Zn^{2+} sensor.

2.0 MATERIALS AND METHODS

2.1 Molecular cloning

pcDNA3.1 plasmid was used for expression of vectors in HeLa cells and pBAD plasmid was used for bacterial expression. Localization of endoplasmic reticulum sensors was done either through a N-terminal signal sequence from cartilage oligomeric matrix protein (COMP) and a C-terminal KDEL sequence, or through the plasma membrane targeted pDisplay plasmid modified with a C-terminal cytoplasmic KKYN ER recycling motif.

2.2 Development of mutant library

Site directed mutagenesis (SDM) was done using primer libraries containing NNK and MNN sequences. Amplification of plasmids using these primers resulted in a random amino acid at the NNK/MNN mutation site. SDM and molecular cloning was done using either PfuUltra II Fusion High-fidelity DNA Polymerase or 2x VeriFi DNA polymerase, following the manufacturers protocol. For non-SDM cloning, restriction digest was used to clone inserts (such as adding KDEL to GZnP3) into plasmids. Plasmid sequence was confirmed with Sanger Sequencing.

2.3 Bacterial lysate screen

SDM products were transformed using Top10 *Escherichia coli* competent cells and plated on agar plates containing 100µg/mL ampicillin. Colonies were picked and incubated overnight at 37°C, 250rpm, in 1mL LB in a deep 96-well plate with 100µg/mL ampicillin and 0.001% arabinose. Bacterial cultures were spun down at 2250g for 5min. After discarding the supernatant, 300uL of BPER buffer with protease was added to the pellets. Pellets were resuspended by placing the 96-well plate on a shaker at room temperature and shaking at 1000rpm for 6min. The resuspended bacteria were kept on the shaker for 2hr at 300rpm to lyse the cells. Debris was pelleted by centrifugation at 2250g for 5min. Lysates were transferred to a new 96-well plate containing TCEP with a final TCEP concentration of 1mM. Lysates were divided amongst two new 96-well plates. Baseline fluorescence of each plate was measured with a Tecan plate reader (Ex: 568nm, Em: 592nm). After a baseline reading, one plate 135µM buffered Zn^{2+} added and one plate had 100µM TPEN added. At 5min and 20min post Zn^{2+} / TPEN addition, the plates were read again using the same imaging settings. Dynamic range was determined by $(Zn^{2+}{}_{(5min\ /\ 20min)} / Zn^{2+}{}_{baseline}) / (TPEN_{(5min\ /\ 20min)} / TPEN_{baseline})$.

2.4 *In situ* Zn^{2+} response curves

HeLa cells were plated on imaging dishes and transfected using PEI and 1250ug of DNA. 48hr post transfection, the DMEM with 10% FBS was washed off with HHBSS buffer (containing 1.26mM Ca^{2+}) and imaged at room temperature with either a 10sec or 20sec time interval. 5min after the beginning of acquisition, 100µM TPEN (unless otherwise

stated) was added to the imaging buffer. 5min after TPEN treatment, the TPEN was washout out with HHBSS (3min time period) then 100µM Zn^{2+} + 2.5µM PTO (unless otherwise stated) was added; acquisition concluded 5min post Zn^{2+} + PTO addition. For imaging analysis of some GZnP-ER experiments, HHBSS buffer without Ca^{2+} was used. Baseline was determined by taking the average, stable, fluorescence of each sensor before the addition of TPEN. Dynamic range was determined by taking the average of the stable maximum fluorescence and dividing by the average of the minimum fluorescence.

2.5 Imaging acquisition and analysis

Imaging experiments using HeLa cells were recorded on a Nikon/Solamere CSUX1 spinning disc microscope 48hr post transfection. Images were captured at either 40x 1.3 NA oil objective or 20x air objective and used MicroManager software to collect imaging data. Both 488nm and 514nm lasers were used at 10% power with a 100ms exposure time. Data was processed using Fiji (ImageJ) using the Time Series Analyzer V3 plugin and StackReg plugin to adjust for x-y drift when needed.

3.0 DEVELOPMENT OF ER-TARGETED GZnPS

3.1 Endoplasmic Reticulum localized GZnP

There is still debate on whether the luminal ER labile Zn^{2+v} concentration is higher or lower than the labile cytoplasmic Zn^{2+} concentration; in fact, estimations range from 1pM to 5nM (Kambe et al. 2015). Previous work done to estimate the labile Zn^{2+} concentration in the lumen of the ER has not made use of single FP Zn^{2+} sensors. This is a limitation of previous studies due to single FP Zn^{2+} sensors having a higher dynamic range, faster kinetics, and the expression of only one FP instead of two (compared to FRET sensors). Because of this, we wanted to localize our current GZnP sensors to the ER.

The simplest way to do this was to fuse an ER SS to target our GZnPs to the ER and a KDEL retention sequence to localize our GZnPs to the lumen of the ER. The SS of COMP, a secretory protein that has been studied in HeLa cells (Crevenna et al. 2016), was fused to the N-terminal of GZnP-1 and -3, and a KDEL retention sequence was fused to the C-terminus of GZnP1 and -3; a flexible linker was placed between GZnP and both the SS and KDEL. These constructs were named GZnP-ERs. When we express our new GZnP-ERs in HeLa cells we see, instead of a diffuse cytoplasmic signal, a reticular ER staining (Fig. 1A)

In addition to GZnPs with a SS and KDEL, we designed a GZnP-ER that is fused to a transmembrane protein as oppose to being luminally expressed in the ER in the case that the luminal sensor did not function as expected. This was done using a pDisplay plasmid that normally localizes to the plasma membrane, but with the addition of a cytoplasmic KKYN recycling motif to be retained in the ER (Zerangue et al. 2001) (Fig. 1B), which we named GZnP3-KKYN.

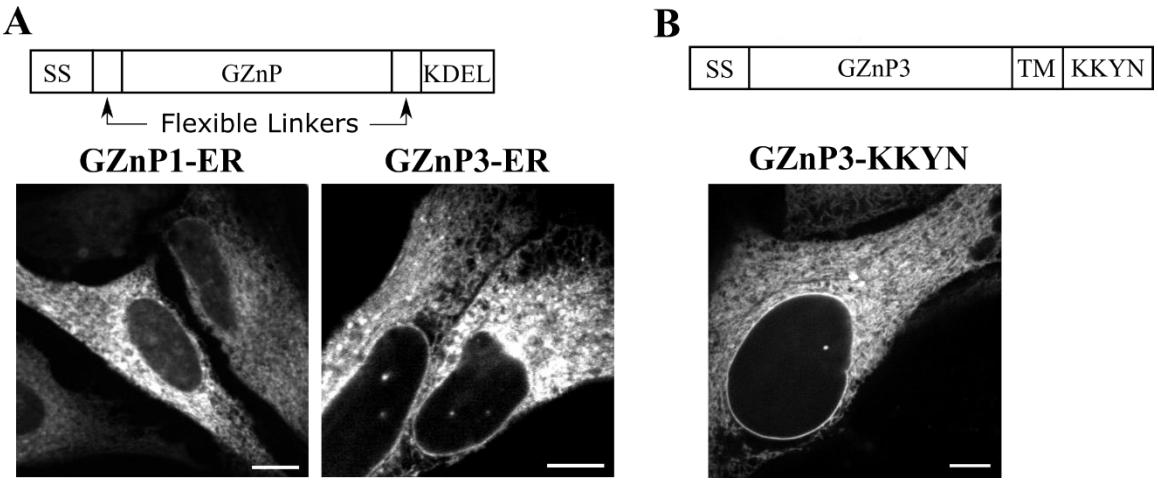

Figure 1. Localization of GZnP-ER. (A) Schematic of GZnP-ER - SS = signal sequence - and localization of GZnP1-ER and GZnP3-ER in HeLa cells. (B) Schematic of GZnP3-KKYN – TM = transmembrane domain – and localization of GZnP3-KKYN in HeLa cells. (Scale bars are 10μm, all images of are Zn^{2+} saturated sensors).

3.2 Characteristics of GZnP-ER

We began or analysis of our new GZnP-ERs with testing their response to Zn^{2+} in HeLa cells. We saw that for both GZnP1- and 3-ER, there was no obvious response to TPEN (Fig. 2A, B). This is not unexpected as if the ER contains a low concentration of labile Zn^{2+}, we may not see a decrease in signal even after TPEN treatment.

To test whether we could still detect a decrease in signal using our new GZnP-ER sensors, we saturated the sensor with Zn^{2+} before adding 100μM TPEN. Surprisingly, we noticed an ~14.5min delay, as oppose to an instant response seen in GZnP3, in signal reduction in GZnP3-ER (Fig. 2C, D).

Along with a delayed TPEN response, we see a significant reduction in dynamic range compared to cytoplasmic GZnP3, this same trend is seen in GZnP1-ER (Fig. 2E). We also noticed a significant increase in baseline fluorescence of GZnP3-ER, but not GZnP1-ER, compared to their cytoplasmic versions (Fig. 2F).

Thus far, our GZnP-ER sensors appear to have varied baseline fluorescence compared to the cytoplasmic sensors, but more importantly, we see a large decrease in dynamic range and a delayed response to TPEN. Because of this, we sought to optimize our GZnP-ER sensors so they behave similar to our cytoplasmic GZnPs.

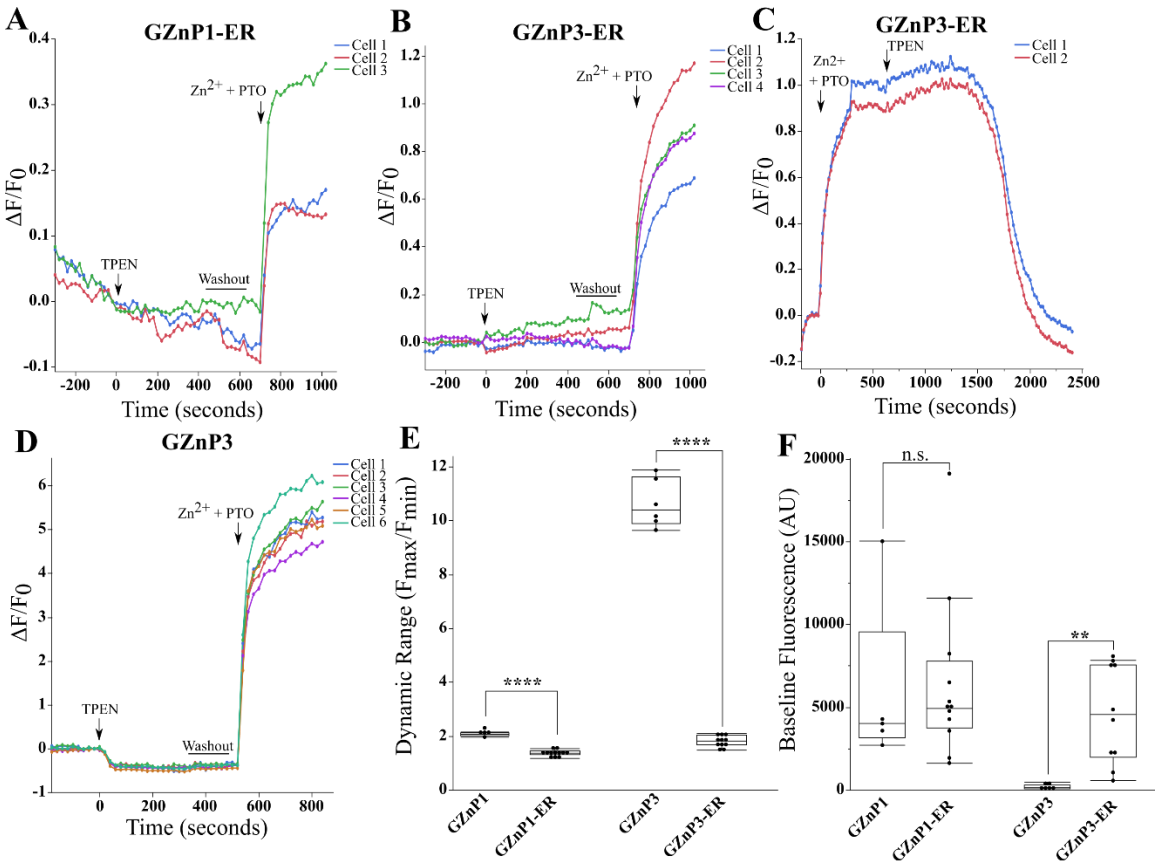

Figure 2. Zn^{2+} response curve of GZnP1- and 3-ER. In Hela cells: Zn^{2+} response curves of GZnP1-ER (A) and GZnP3-ER (B). Zn^{2+} response curve of GZnP3-ER with Zn^{2+} + PTO added before TPEN (C) and GZnP3 (D). Dynamic range (E) and baseline fluorescence (F) comparison of GZnP1- and 3-ER to the cytoplasmic GZnP1 and GZnP3. (Two tailed T-test. ** = $p<0.01$, **** = $p<0.0001$).

3.3 Functionality of GZnP-KKYN

Due to the delayed response of GZnP3-ER to TPEN, we were worried that the sensor was nonfunctional, so we began to troubleshoot this first. We thought that TPEN may not be as effective at chelating Zn^{2+} in the ER compared to the cytoplasm, so we added 5μM PTO with TPEN so the Zn^{2+} would be brought out of the ER by PTO, then bound by TPEN. When we did this, we found that after about a 5min delay, as oppose to ~14.5min, we could see a decrease in signal of GZnP3-ER after Zn^{2+} saturation (Fig. 3A). Although this was an improvement, it was not an instant reduction in signal like we see in GZnP3.

We then tested our GZnP3-KKYN to see if it behaved similarly to GZnP3-ER. Doing the same treatments as in figure 3A, we see that GZnP3-KKYN behaved very similarly to GZnP3-ER (Fig. 3B). GZnP3-KKYN still showed a delayed reduction in signal when treated with TPEN + PTO, and it showed a similar increase in baseline fluorescence and reduced dynamic range compared to GZnP3 (Fig. 3C, D).

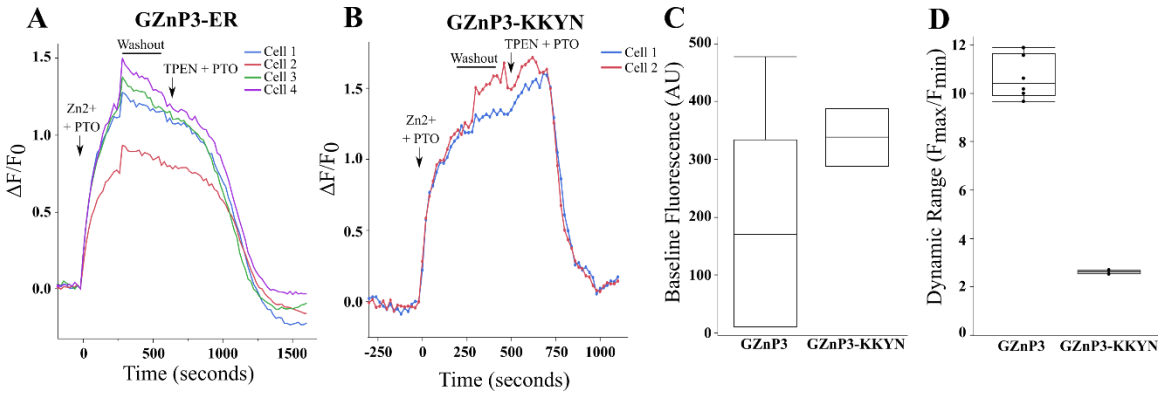

Figure 3. Zn^{2+} response curve of GZnP3-KKYN. In HeLa cells: (A) Zn^{2+} response curve of GZnP3-ER using 100µM TPEN + 5µM PTO to chelate labile Zn^{2+}. (B) Zn^{2+} response curve of GZnP3-KKYN in HeLa cells using 100µM TPEN + 5µM PTO. Baseline fluorescence (C) and dynamic range (D) of GZnP3-KKYN compared to GZnP3. (D).

3.4 Optimizations of GZnP-ER

With the minor improvements in reducing the signal of GZnP-ER using TPEN + PTO, we next focused on improving the overall dynamic range of the sensor. First, we tried removing the linker region between GZnP3 and KDEL (Fig. 4A) to see if the dynamic range was improved. After addition of Zn^{2+} + PTO, it appeared that the dynamic range was not improved.

Because GFP can form di-sulfide bond oligomers in the ER (Aronson, Costantini and Snapp 2011), we decided to test the response to Zn^{2+} of our GZnP3-ER sensor in the presence of various reducing agents. We reasoned if there are GZnP3-ER sensors forming aggregates in the ER, they may not be responding to Zn^{2+} but still be fluorescent, increasing the background fluorescence seen while imaging (Fig. 4B-E). None of the reducing agents tested increased the dynamic range, nor solved the delay in response to TPEN, of GZnP3-ER to a comparable range as GZnP3 (Fig 4F).

We also developed a GZnP3 that contains a C-terminal flexible linker and KAAL sequence to mimic GZnP3-ER but be expressed in the cytoplasm to determine if the additional fused residues on the C-terminal of GZnP3-ER was causing the reduction of dynamic range. After testing the construct in HeLa cells, we see that it behaves very similar to GZnP3, indicating that additional residues on the C-terminus of our sensors does not affect its function (Fig 5A-C).

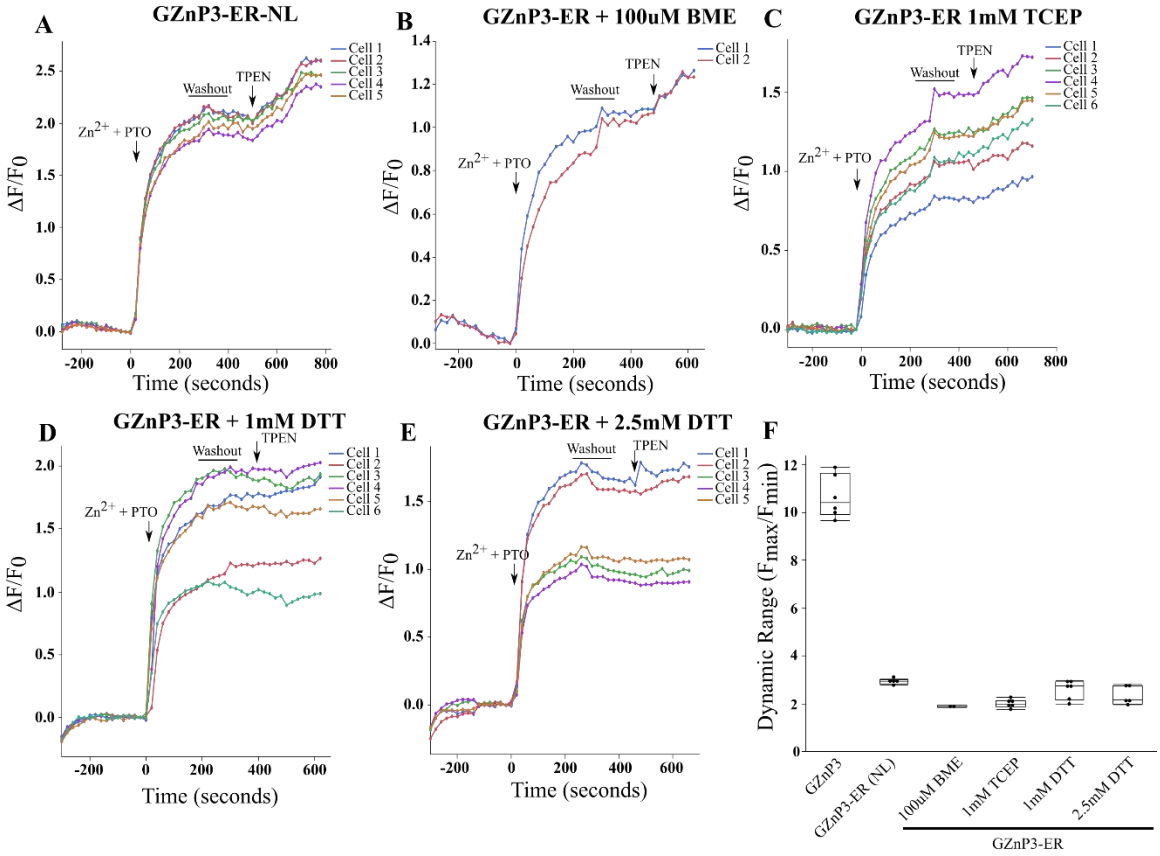

Figure 4. Optimizations of GZnP3-ER. In HeLa cells: (A) Response to Zn^{2+} + PTO of GZnP3-ER-NL (No Linker between GZnP3 and KDEL). Response to Zn^{2+} + PTO of GZnP3-ER in the presence of 100μM BME (B) or 1mM TCEP (C). GZnP3-ER response to Zn^{2+} + PTO in the presence of 1mM DTT (D) or 2.5mM DTT (E). (F) Quantification of dynamic ranges of GZnP3-ER and GZnP-ER-NL from A-E.

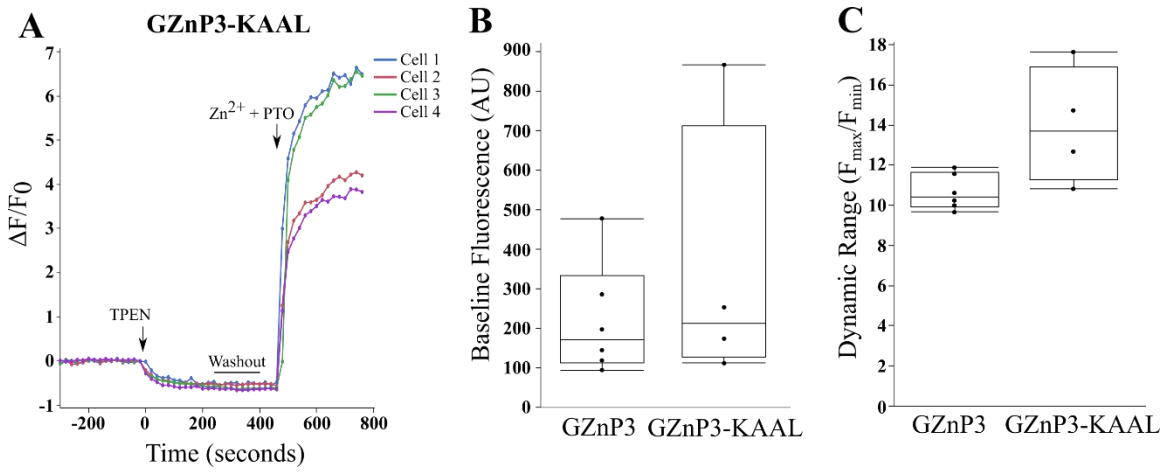

Figure 5. Zn^{2+} response curve of GZnP3-KAAL. In HeLa cells: (A) Zn^{2+} response curve of GZnP3-KAAL. Baseline fluorescence (B) and dynamic range (C) of GZnP3-KAAL compared to GZnP3.

3.5 GZnP-ER in 0Ca^{2+} HHBSS buffer

After no improvements of dynamic range were found, we turned back to the issue of the delayed TPEN response, this time, with a new hypothesis. It was hypothesized that the weak response of our GZnP-ERs to TPEN could be because TPEN was chelating not only Zn^{2+} in the ER, but also calcium, as TPEN does bind calcium in addition to Zn^{2+} (Stork and Li 2006). Because ER calcium concentrations can be up to 800µM (Samtleben et al. 2013), we thought the TPEN could be chelating calcium before Zn^{2+}. To test this, we removed the calcium from our HHBSS buffer to reduce the amount of calcium in the assay. When we did this, we found that we can get an almost immediate decrease in saturated GZnP3-ER signal with TPEN addition (Fig 6A). With this discovery, we began to use our high affinity GZnP1-ER and our low affinity GZnP3-ER to see if we can estimate the concentration of labile Zn^{2+} in the ER.

We began by comparing the Zn^{2+} response of both GZnP1-ER and GZnP3-ER in our 0Ca^{2+} HHBSS buffer. We found that, using TPEN, we can get a reduction from baseline of GZnP1-ER, but not GZnP3-ER (Fig. 6B, C); this suggests that there is a lower concentration of labile Zn^{2+} in the ER compared to the cytoplasm because we are able to get a reduction of signal from baseline of GZnP3 but not GZnP3-ER. Interestingly, when we use a weaker Zn^{2+} chelator, TPA (10pM K_d for Zn^{2+}), we do not see a reduction of signal from baseline in either GZnP1-ER nor GZnP3-ER (Fig. 6D, E); this again suggests that the labile Zn^{2+} concentration is low, as a chelator with 10pM affinity is not strong enough to give a detectable reduction of labile Zn^{2+} in the ER.

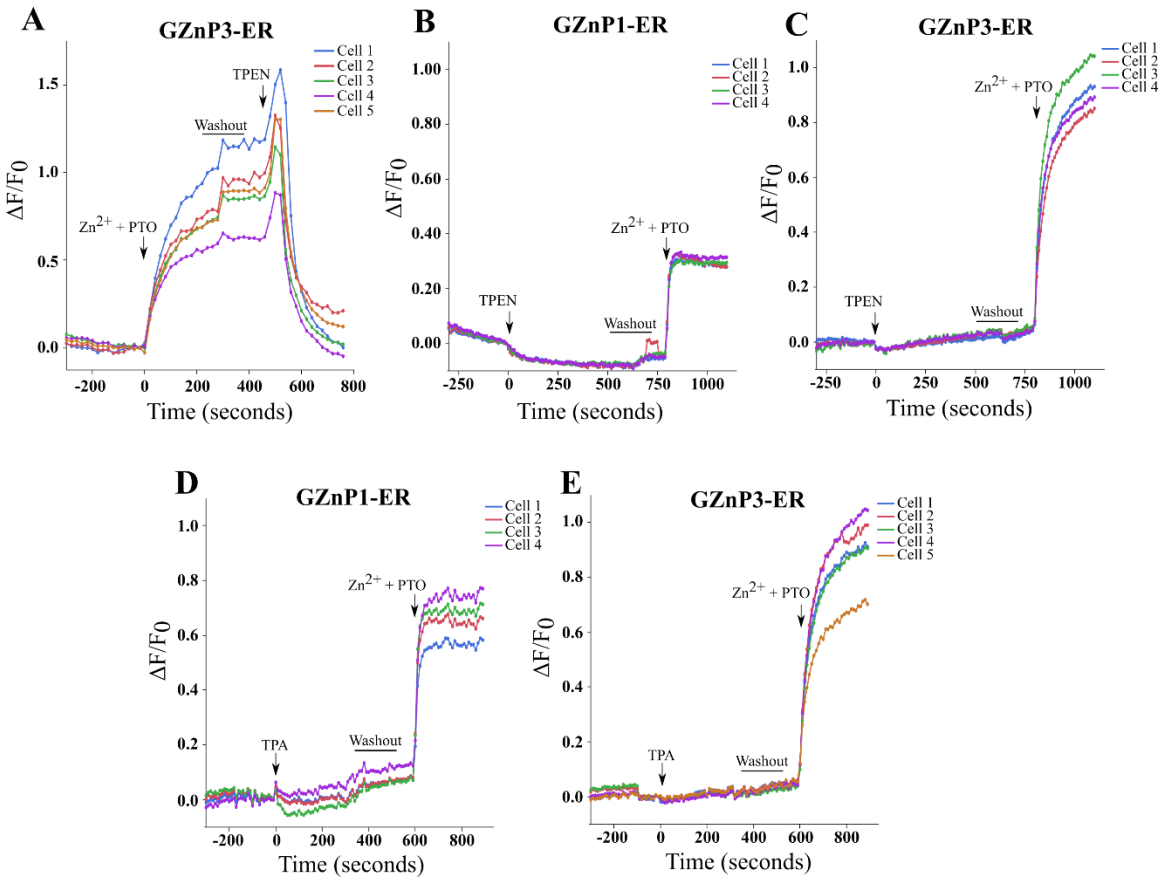

Figure 6. GZnP-ER in 0Ca^{2+} HHBSS buffer. (A) Zn^{2+} response curve of GZnP3-ER in HeLa cells in 0Ca^{2+} HHBSS buffer. Zn^{2+} response curves using TPEN (B,C) or TPA (D,E) of GZnP1-ER (B,D) and GZnP3-ER (C,E).

3.6 Influx of labile Zn^{2+} from the cytoplasm to the ER

Finally, we tested to see if the addition of only PTO can result in an increase of signal from baseline in GZnP1-ER. In theory, if there is a higher concentration of labile Zn^{2+} in the cytoplasm, then the PTO will shuttle the Zn^{2+} down the concentration gradient from the cytoplasm to the ER. When adding 5μM PTO to HeLa cells expressing GZnP1-ER, we see an immediate increase in signal from baseline (Fig. 7A). This signal was further increased by the addition of Zn^{2+}. To confirm that the increase in signal in the ER was from intracellular Zn^{2+}, we performed the same experiment, except we treated the cells with TPEN first to chelate away any intracellular Zn^{2+}. When we did this, we found that the addition of 5μM PTO did not increase the signal of GZnP1-ER, only after the addition of Zn^{2+} did the signal increase (Fig. 7B). This data suggests that the labile concentration of Zn^{2+} in the ER is at least lower than that of the cytoplasm.

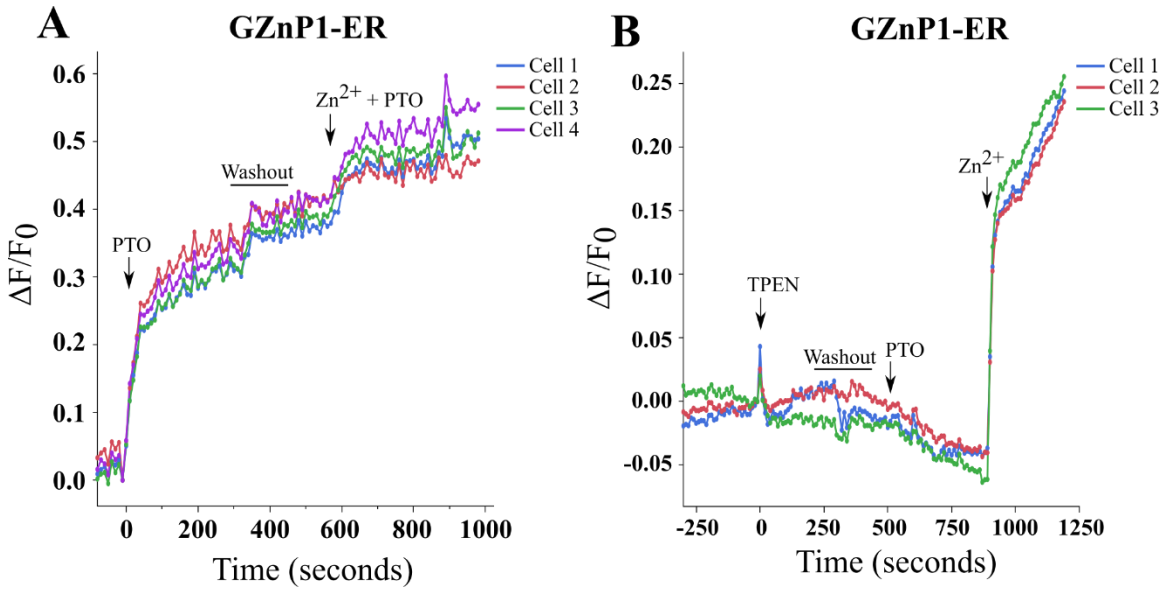

Figure 7. Zn^{2+} diffusion into the ER. In Hela cells: (A) GZnP1-ER with 5µM PTO added first. (B) GZnP1-ER with 5µM PTO after chelating intracellular Zn^{2+} with TPEN.

4.0 DEVELOPMENT OF RED FLUORESCENT Zn^{2+} PROBES

4.1 FustionRed-RZnP and mRuby-RZnP

Red fluorescent Zn^{2+} sensors use the same format as the develop GZnPs; with to a cpFP flanked by two ZFs (Fig. 8A). When developing a new fluorescent Zn^{2+} sensors, we wanted to test cpFPs that have been used in fluorescent Ca^{2+} sensors and that were also pH resistant. The two candidate cpFPs were cpFusionRed and cpmRuby (Dana et al. 2016, Shen et al. 2018b). When testing an early prototype of a RZnP that uses cpFusionRed (FR-RZnP), we see that the sensor does not respond to either TPEN or Zn^{2+} + PTO (Fig. 8B). Similar to FR-RZnP0.1, none of the other FR-RZnP prototypes or a prototype cpmRuby sensor responded to TPEN or Zn^{2+} + PTO. All RZnPs using either cpFusionRed or cpmRuby had cells with baseline fluorescence that were near background levels (Fig. 8C). Because these prototype sensors showed poor response to Zn^{2+}, we did not continue optimizing these sensors, but the success of developing cpFusionRed and cpmRuby Ca^{2+} sensors suggests that they might be good candidates for creating the first generation red Zn^{2+} sensors that are resistant to pH changes.

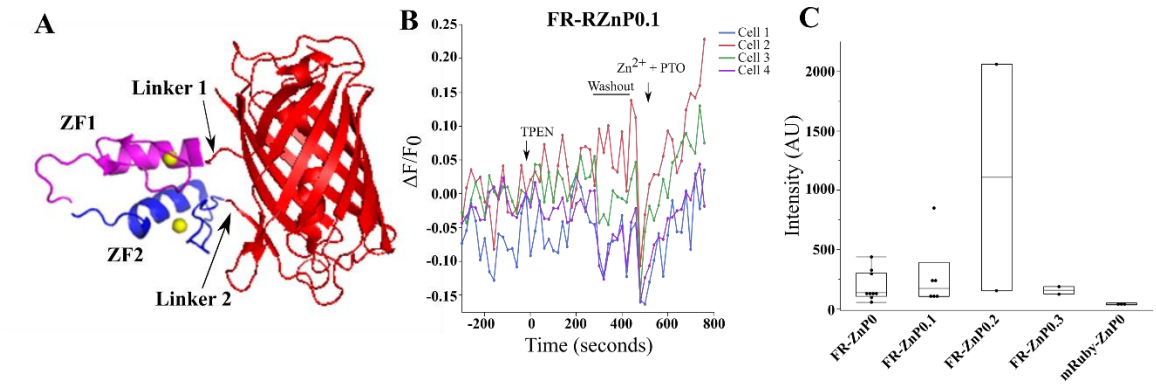

Figure 8. Zn^{2+} response curves of FR-ZnP and mRuby ZnP in Hela cells. (A) Schematic of a red fluorescent Zn^{2+} probe. ZF1 and ZF2 are zinc fingers 1 and 2, respectively, and the linker regions are the peptide sequences connecting the ZFs to the cpFP. (B) Representative Zn^{2+} response curve of FR-ZnP0.1. (C) Baseline fluorescence of all RZnPs using either cpFusionRed (FR-RZnPs) or cpmRuby (mRuby-ZnP0).

Although cpFusionRed and cpmRuby showed little promise for developing red sensors, prototype sensors using a cpmApple have been previously made that can respond to changes in Zn^{2+}. The caveat to cpmApple is that its pKa is ~6.5, which is higher than cpEGFP, making it more prone to changes in pH (Gandasi et al. 2015).

One of the prototype sensors made using cpmApple is RZnP0.41. It's dynamic range is ~2.0. The major issue with RZnP0.41 is that the response to Zn^{2+} is very unstable (Fig. 9A). After Zn^{2+} saturation, the signal decays to F_{min} in ~160 seconds. Another cpmApple-based protype sensor shows a stable response to Zn^{2+}; however, RZnP0.81 has a dynamic range of ~1.2 (Fig. 9B). Baseline fluorescence, defined as fluorescence of the sensor at resting conditions, and dynamic ranges of the sensors are shown in figure 9C and 9D

Both sensors above are good candidates for further mutagenesis to produce a sensor that has at least a high dynamic range, modest brightness, stable response to Zn^{2+} and fast kinetics. Currently, neither sensor is a good candidate for bacterial *in vitro* screens that have been used to develop GZnP sensors in our lab (Fudge et al. 2018, Minckley et al. 2019). Addition of Zn^{2+} would not be detected in RZnP0.41 due to the rapid decrease in signal after Zn^{2+} saturation, and the dynamic range of RZnP0.81 is too small to be detected above the variance seen in the bacterial lysate screen. Because of this, both sensors underwent single-site mutagenesis where only one amino acid was mutated, resulting in mutant libraries of 20, and screened *in situ*.

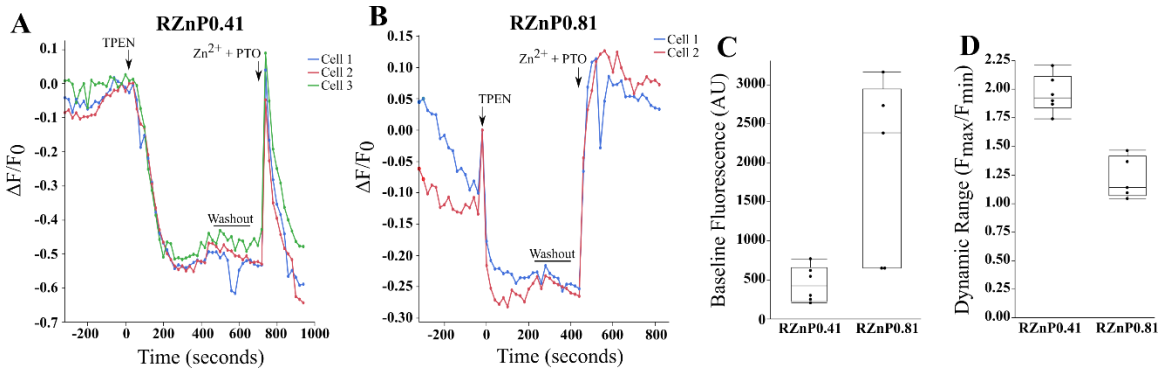

Figure 9. Zn^{2+} response curves of RZnP0.41 and RZnP0.81 in HeLa cells. Representative Zn^{2+} response curve of RZnP0.41(A) and RZnP0.81 (B). Baseline fluorescence(C) and dynamic range(D) of RZnP0.41 and RZnP0.81.

4.2 Mutagenesis of RZnP0.81 residues 35, 36, and 281

Initially, we focused on improving RZnP0.81, and to do this, we targeted amino acids in the linker regions of RZnP0.81. Mutations of amino acids were done through SDM. RZnP0.81 mutants that were tested in HeLa cells showed either no response to TPEN and Zn^{2+} + PTO or had an unstable response to Zn^{2+} + PTO, similar to what is seen in RZnP0.81. An example of a non-responsive sensor, RZnP0.81 G36P, is shown in figure 10A and an example of a mutant with an unstable response, RZnP0.81 R35G-G36V-A281P, is shown in figure 10B. When looking at the baseline fluorescence (Fig. 10C) and dynamic range (Fig. 10D) of all mutants tested *in situ*, we see there is no improvement over RZnP0.81 of any of the mutants tested.

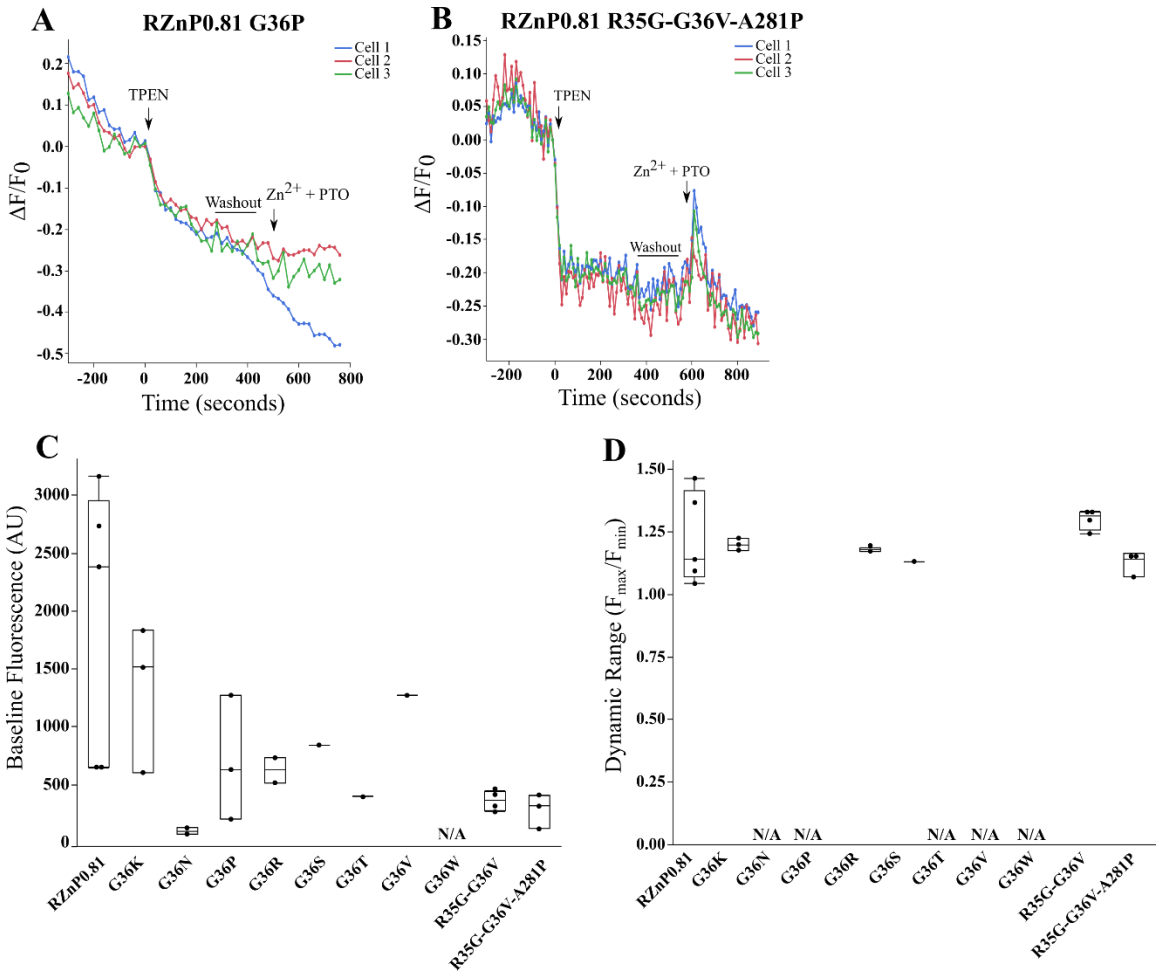

Figure 10. Zn^{2+} response curves of RZnP0.81 with linker 2 mutations in HeLa cells. (A) Representative trace of a mutant, RZnP0.81 G36P, that has no response to Zn^{2+} + PTO. (B) Representative trace of a mutant, RZnP0.81 R35G-G36V-A281P, that has an unstable response to Zn^{2+} + PTO. Baseline fluorescence (C) and dynamic range (D) of 10 RZnP0.81 mutants. N/A indicates mutants that did not fluoresce or respond to Zn^{2+} + PTO.

4.3 Mutagenesis of RZnP0.81 at residue 33

After no success mutating positions 35, 36, or 281 in RZnP0.81, mutations in position 33 were tested. This is due to position 33 being a crucial residue that was mutated in improvement of our GZnP sensor (Fudge et al. 2018, Minckley et al. 2019).

Interestingly, some mutants tested appeared to be putative high affinity sensors, such as RZnP0.81 Y33C (Fig. 11A). This is seen by the addition of Zn^{2+} + PTO not producing signal above the baseline, suggesting that the sensor is saturated with Zn^{2+} at ~100pM labile Zn^{2+}. RZnP0.81 Y33C appears to also has a slightly unstable response to the addition of Zn^{2+} + PTO. Using the criteria of putative high-affinity sensors, we can determine if other mutants tested are potential high-affinity sensors, which is shown in figure 11B.

Although some high-affinity sensors may have been produced, we see a noticeable decrease in baseline fluorescence of all mutants tested (Fig.11C). However, the dynamic range of almost all mutants are comparable to RZnP0.81 (Fig. 11D).

Higher affinity RZnP mutants are desirable due to the low concentration of labile Zn^{2+} in the cytoplasm and the even lower concentrations of labile Zn^{2+} in some intracellular compartments, such as the mitochondria and ER (Qin et al. 2011). The putative high affinity sensors can potentially be used to create the first generation of high affinity RZnPs.

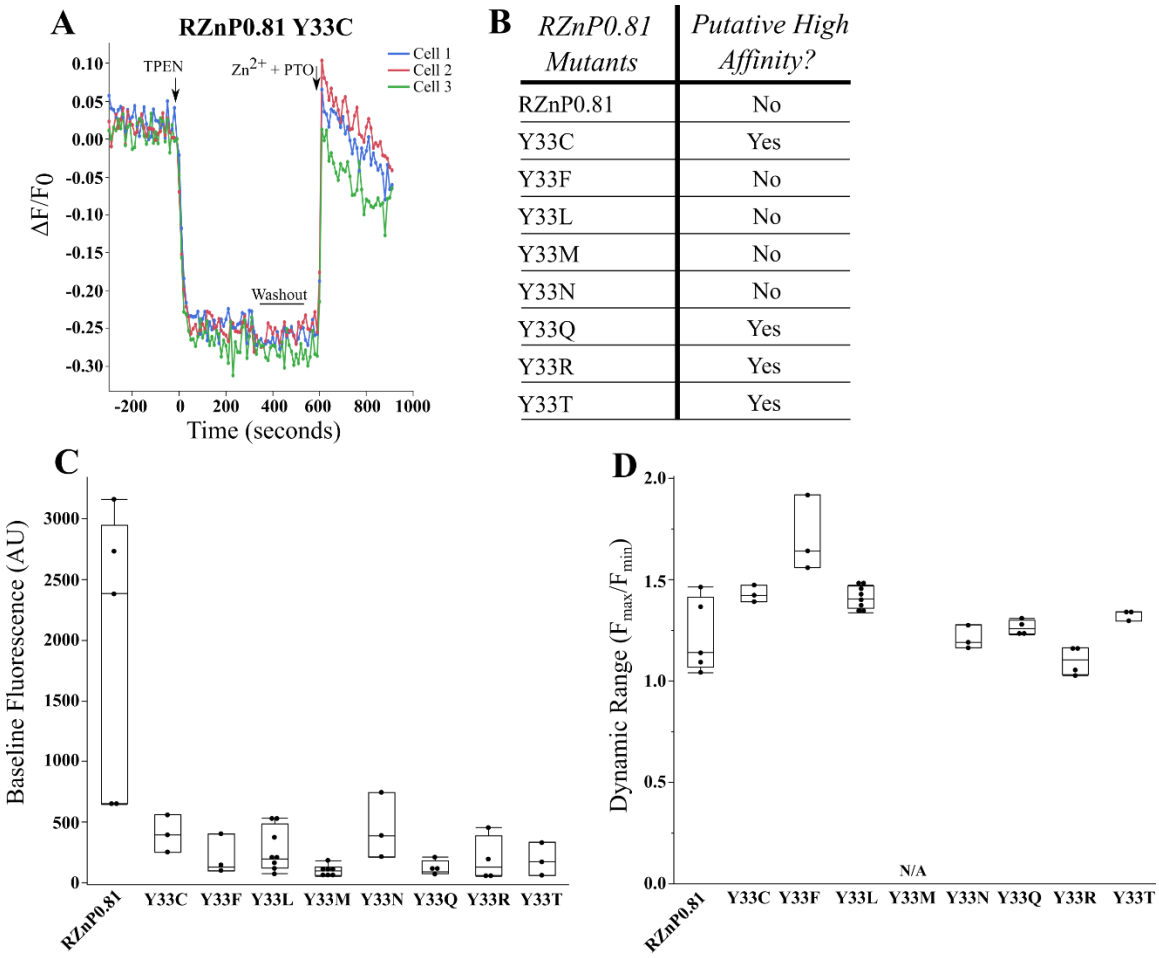

Figure 11. Zn^{2+} response curves of RZnP0.81 with residue 33 mutations in HeLa cells. (A) Representative Zn^{2+} response curve of the putative high affinity RZnP0.81 Y33C. (B) Table of putative high affinity RZnP0.81 mutants. Baseline fluorescence (C) and dynamic range (D) of RZnP0.81 mutants at position 33. N/A represents sensors that did not respond to Zn^{2+} + PTO.

4.4 RZnP0.81 Y33C bacterial lysate screen

Because RZnP0.81 Y33C has the highest dynamic range of the putative high affinity sensors, it was selected for a bacterial lysate screen observing mutations in position 34, another residue that was key to the improvement of our GZnPs (Fudge et al. 2018, Minckley et al. 2019). As mentioned previously, RZnP0.81 is not a good candidate for the lysate screen, however, we wanted to see if we could successfully screen for a RZnP with a high dynamic range that maintained the putative high affinity of RZnP0.81 Y33C.

Upon screening 46 mutant colonies in position 34, we found some colonies had an almost ~50% increase in dynamic range 20min after addition of Zn^{2+} and TPEN (Fig. 12A). These mutants were cloned into pcDNA3.1 to be expressed and tested in HeLa cells; the mutants were found to be H34P, H34S. H34T, and H34Y. The only mutant to have a comparable dynamic range to the parent sensor was H34T, however, it appeared this mutant was not a putative high affinity Zn^{2+} sensor (Fig. 12B).

Upon analysis of dynamic ranges of the other mutants (Fig. 12C), we see the H34P and H34Y mutations did not have a detectable response to Zn^{2+} + PTO, while the H34S mutant only showed a weak response to Zn^{2+} + PTO. This indicates that RZnP0.81 Y33C is not a good candidate for a parent sensor in the bacterial lysate screen.

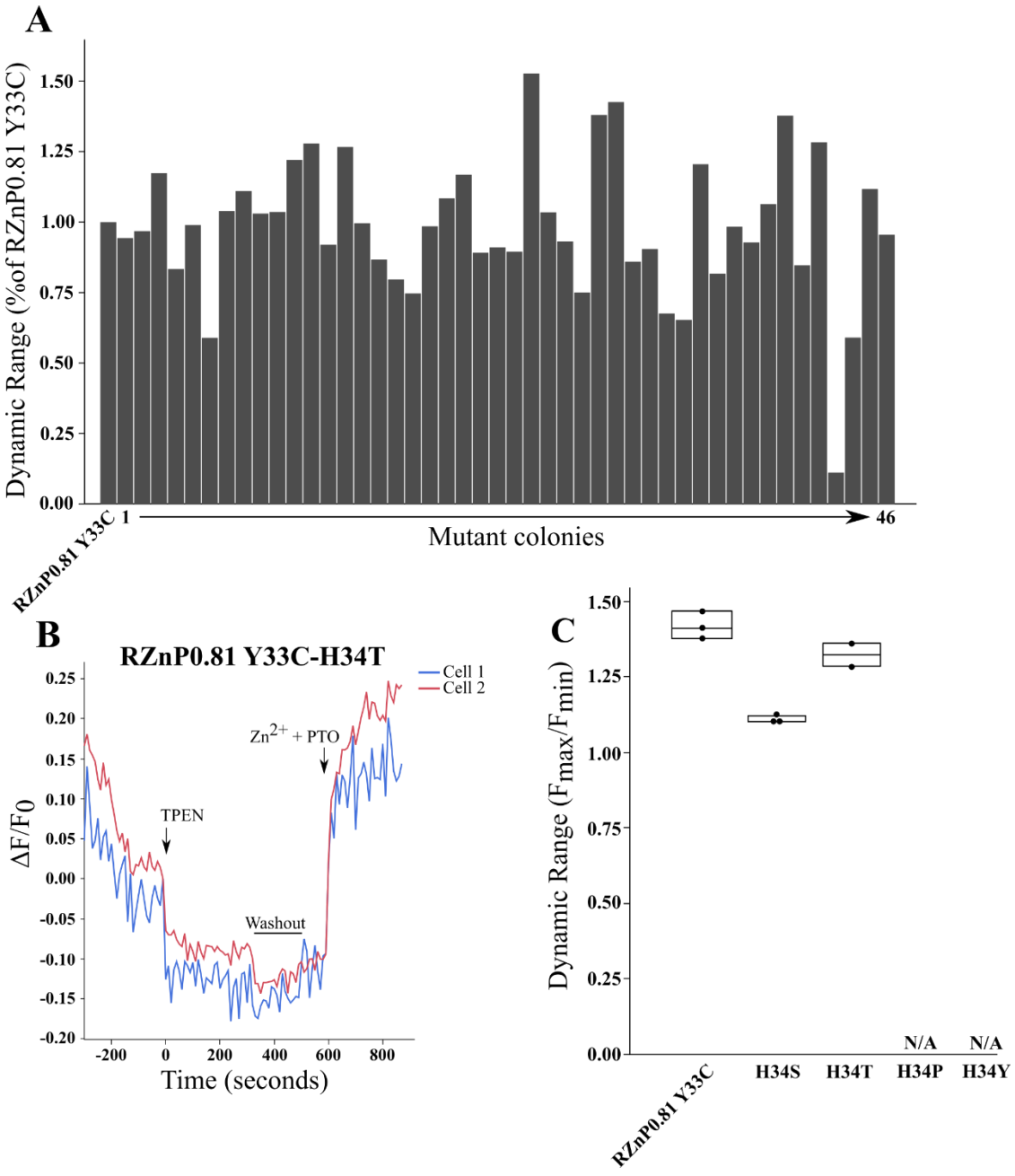

Figure 12. RZnP0.81 Y33C bacterial lysate screen with H34 mutations. (A) Dynamic range as %of RZnP0.81 Y33C 20min post Zn^{2+} and TPEN treatment. Bars 1 to 46 represent individual colonies that were tested. (B) RZnP0.81 Y33C-H34T Zn^{2+} response curve in HeLa cells. (C) Dynamic range of screened mutants in HeLa cells.

4.5 RZnP0.41 mutagenesis

Along with optimization of RZnP0.81, we also wanted to optimize RZnP0.41. The first goal was to create a RZnP0.41 that has a stable response after saturation with Zn^{2+}. To begin, position 36, a serine residue, underwent SDM. This is one of the two residues in linker 2 that is different from RZnP0.81. One sensor tested, RZnP0.41 S36V, showed increased stability to the addition of Zn^{2+} + PTO compared to RZnP0.41 (Fig. 13A, B).Of the ten amino acids tested, none appeared to have an improved dynamic range compared to RZnP0.41 (Fig. 13C). Because RZnP0.41 S36V showed improved stability, this sensor was selected to be a new parent RZnP sensor, named RZnP0.41.1, and mutated to further improve its stability.

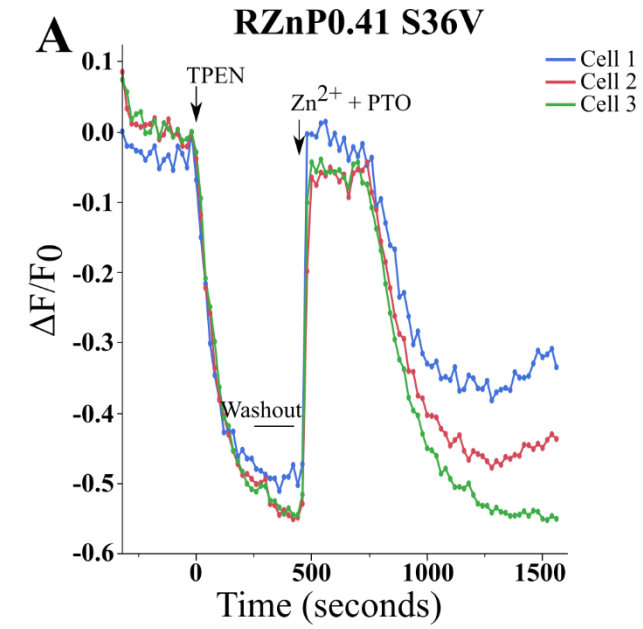

B

RZnP0.41 Mutants	*Increased Stability?*
RZnP0.41	-
S36E	No
S36I	No
S36K	No
S36L	No
S36Q	No
S36R	No
S36T	No
S36V	Yes
S36Y	No

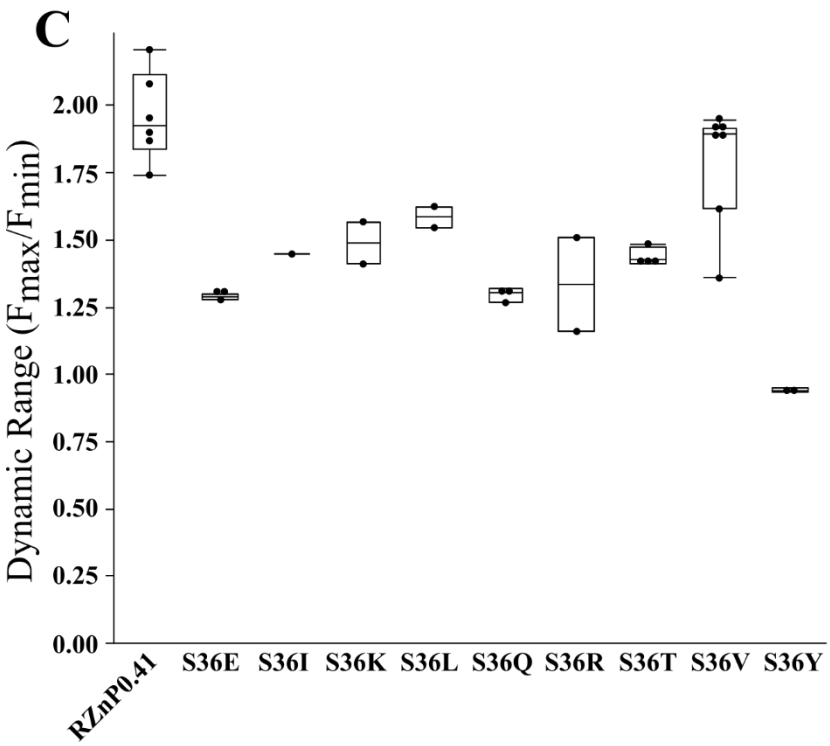

Figure 13. Zn^{2+} response curve of RZnP0.41 with mutagenesis at position 36 in HeLa cells. (A) Representative Zn^{2+} response curve of RZnP0.41 S36V. (B) Table indicating whether RZnP0.41 mutants showed improved stability. (C) Dynamic range of RZnP0.41 mutants at position 36.

4.6 RZnP0.41.1 mutagenesis

RZnP0.41.1 subsequently underwent mutagenesis to attempt to create a more stable sensor that retains the ~2 fold dynamic range of RZnP0.41.1. The mutations tested for RZnP0.41.1 were mostly focused on positions 37 (proline) and 38 (valine). No mutations tested in these two regions improved the dynamic range of the sensor (Fig. 14A); in fact, all mutants resulted in a stability decrease when responding to Zn^{2+}.

Due to no improved mutants being developed through linker 2 SDM, we decided to mutate linker 1 from EFKNN to TR; this new sensor was named RZnP0.41.2. The rational for the change of linker 1 comes from R-GECO, one of the original red single FP calcium sensors, that had a TR linker 1 region (Zhao et al. 2011). This sensor, however, was still not an improvement over RZnP0.41.1 (Fig. 14B). The response to Zn^{2+} was highly unstable and the dynamic range was ~1.13 fold.

Although RZnP0.41.2 was not a promising sensor, position 36 of this sensor was mutated due to the success that was seen from RZnP0.41 to RZnP0.41.1. Only a few mutants were tested in this region: arginine, lysine, and leucine. Excitingly, the arginine mutation resulted in a stable response to Zn^{2+} + PTO (Fig. 14C). As for the other mutants, both lysine and leucine showed no increased dynamic range over RZnP0.41.1, but the arginine mutation resulted in an ~1.6 fold dynamic range (Fig. 14D). In addition to the improved stability and dynamic range, the baseline fluorescence is higher than both RZnP0.41 and RZnP0.41.1, making it a good candidate for the bacterial lysate screen. This new sensor was named RZnP0.41.3.

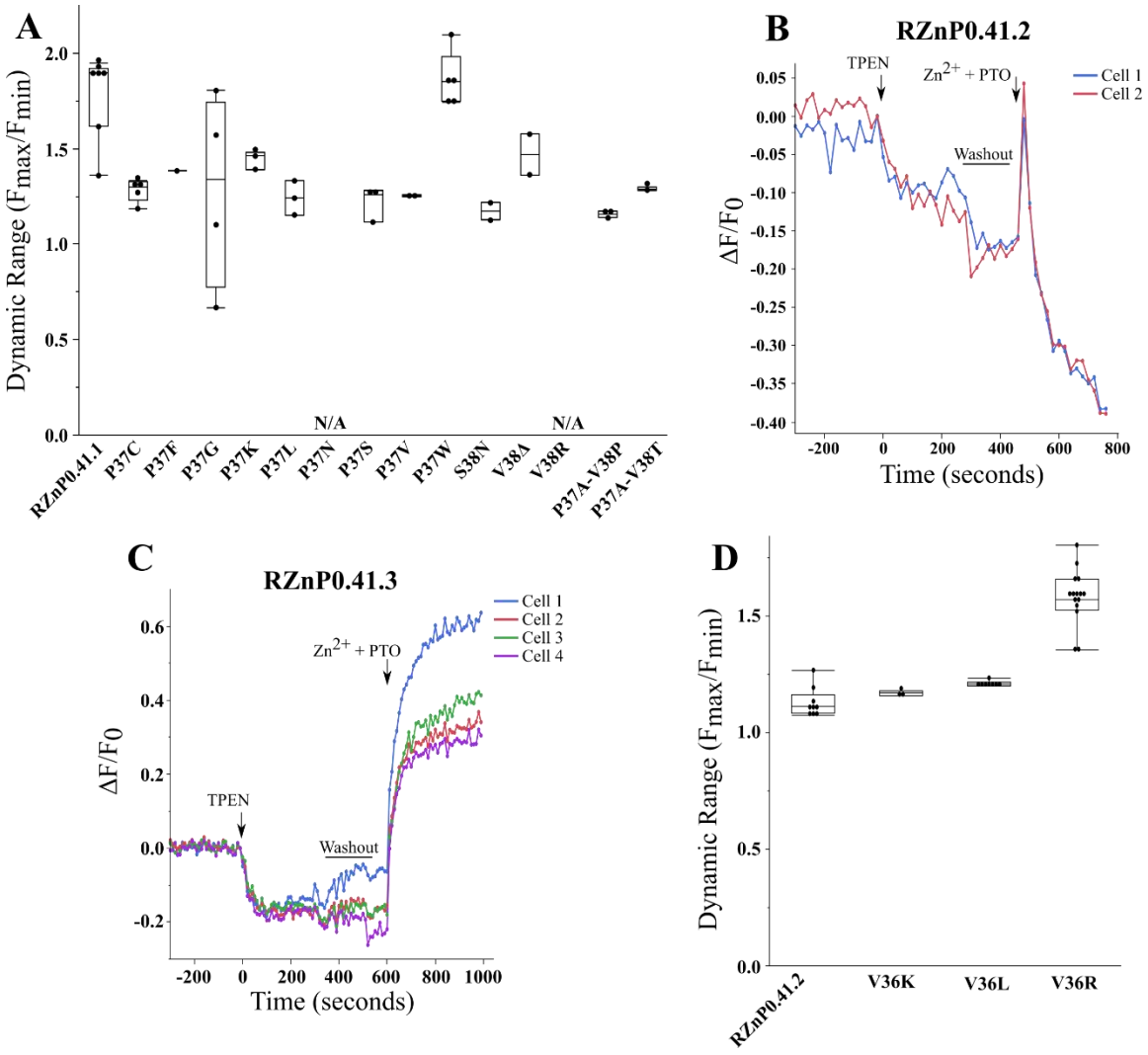

Figure 14. Zn^{2+} response curves of RZnP0.41.1 mutants in HeLa cells. (A) Dynamic ranges of RZnP0.41.1 mutations. N/A represents sensors that did not respond to Zn^{2+} + PTO. (B) Zn^{2+} response curve of RZnP0.41.2. (C) Zn^{2+} response curve of RZnP0.41.3. (D) Dynamic ranges of RZnP0.41.2 mutations.

4.7 Development of RZnP1

Due to its increased baseline fluorescence and stable 1.6-fold dynamic range, RZnP0.41.3 was cloned into a bacterial expressing vector to test whether this sensor will be viable for screening *in vitro*. Preliminary results show that the dynamic range of RZnP0.41.3 *in vitro*, 3min and 20min, after addition of Zn^{2+} and TPEN was ~1.6 fold, similar to what is seen *in situ*. Due to the success of the preliminary *in vitro* assay, we performed a double SDM reaction on RZnP0.41.3 at positions 33 and 34, generating a 400 mutant library.

After mutagenesis of positions 33 and 34 in RZnP0.41.3, 485 colonies were tested *in vitro* (Fig. 15A). We established criteria for selecting mutant sensors to test *in situ* to avoid testing too many mutants. The criteria for selecting a mutant to test *in situ* are, the baseline fluorescence of the mutant is comparable to the parent sensor, the dynamic range of a given mutant is similar at 3min and 20min post TPEN and Zn^{2+}, and the dynamic range is at least ~2.5 fold greater than the parent sensor. Using this criteria, 7 mutants were selected to be tested *in situ*.

One mutant, RZnP0.41.3 H34A, shown in figure 15B, displayed a stable response to Zn^{2+} + PTO and a significantly improved dynamic range over RZnP0.41.3, quantification shown in figure 15C.

Looking at all mutants tested, a significant increase in dynamic range over RZnP0.41.3, with some mutants reaching a dynamic range that is more than double that of RZnP0.41.3, is seen (Fig. 15B). On comparison of baseline fluorescence of all the mutants (Fig. 15D), we see that only RZnP0.41.3 T33V-H34A has a significantly higher

baseline fluorescence compared to RZnP0.41.3. However, we see that the RZnP0.41.3 H34A mutant had the highest frequency of above average intensity cells.

Notably, all sensor mutations either have a single mutation in position 34, or a double mutation that has a valine in position 33 (except the T33L-H34L mutant). In addition to this, when comparing the double mutants to their single mutant counterpart (i.e. comparing T33V-H34A to H34A and T33V-H34Q to H34Q), the single mutant has an increased dynamic range.

Because of this, we decided to rationally make an RZnP0.41.3 H34R as the T33V-H34R mutant had one of the highest dynamic ranges of the tested mutants, and we predicted that the single mutant counterpart would have an increased dynamic range. After testing RZnP0.41.3 H34R in HeLa cells, we surprisingly saw a slight, but significant, decrease in dynamic range (Fig. 15E).

Due to its high dynamic range and high frequency of bright cells, RZnP0.41.3 H34A, Zn^{2+} response curve shown in, figure 8E, was currently the best red sensor.

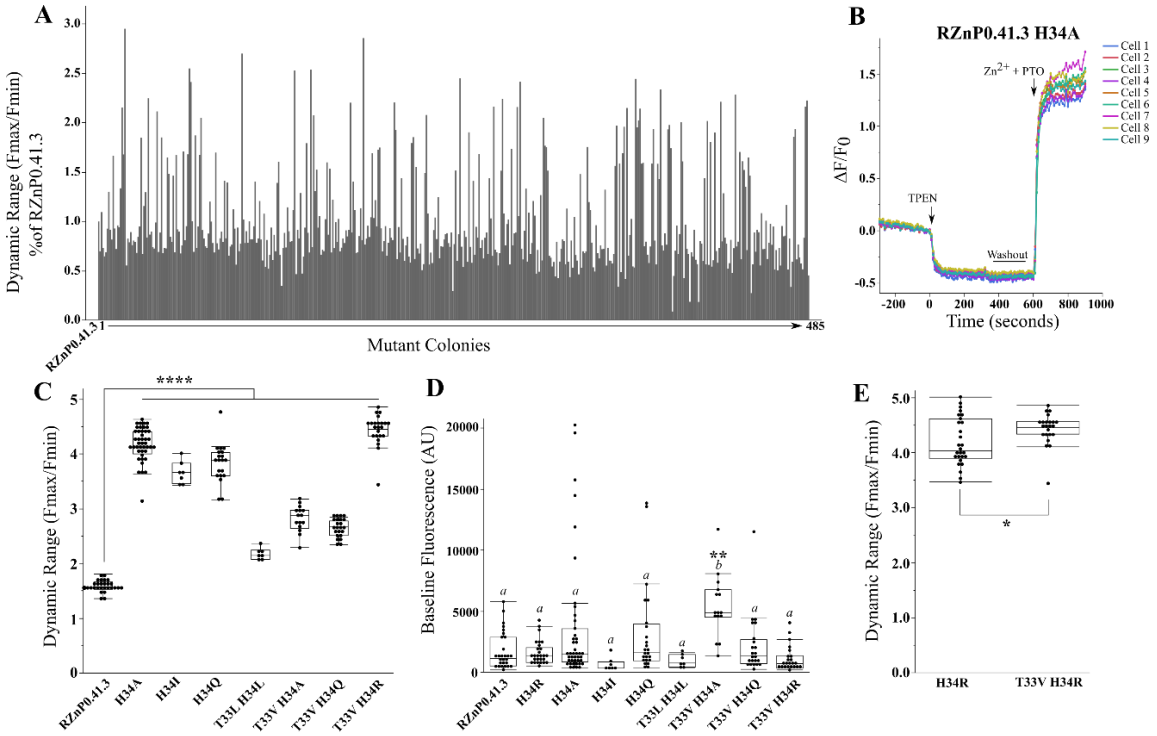

Figure 15. RZnP0.41.3 positions 33 and 34 mutagenesis. (A) Results of the bacterial lysate screen of RZnP0.41.3 mutants represented as %of RZnP0.41.3 dynamic range. (B) Zn^{2+} response curve of RZnP0.41.3 H34A. (C) In HeLa cells: dynamic range of hits from screen in A (One-way ANOVA with Dunnett's Method, **** = $p<0.0001$). (D) Baseline fluorescence of RZnP0.41.3 mutants. Only RZnP0.41.3 T33V-H34A showed a significant increase in baseline fluorescence. (One-way ANOVA with Dunnett's Method, *a* is significantly higher than *b*, no significance between *a's*. ** = $p<0.01$). (E) Dynamic range comparison of RZnP0.41.3 T33V-H34R and RZnP0.41.3 H34R mutants (Student's t-test, * = $p<0.05$).

In addition to rationally testing RZnP0.41.3 H34R, we decided to do a final *in vitro* screen only mutating position 34, as we wanted to ensure we identified the best RZnP0.41.3 mutant in this position. 46 mutant colonies were tested, and many colonies were seen to have the ~2-2.5 fold increase in dynamic range over RZnP0.41.3 (Fig. 16A), this is similar to what was seen previously in the double mutant screen (Fig. 15A). One well from the lysate screen showed over an almost 4-fold increase of dynamic range compared to RZnP0.41.3; this mutant was sequenced and found out to be H34L. Mutants were selected based on the criteria mentioned previously and cloned into pcDNA3.1 to test in HeLa cells. After assessing the dynamic range in HeLa cells (Fig. 16B), no improvement over RZnP0.41.3 H34A was found. We therefore decided that RZnP0.41.3 H34A will be the first generation of red sensors, and named RZnP1.

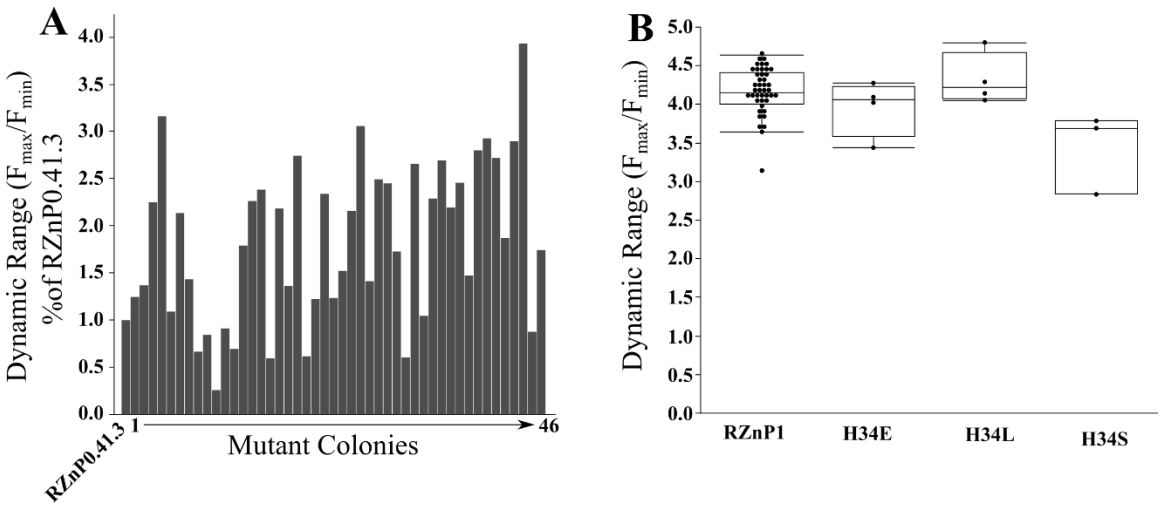

Figure 16. RZnP0.41.3 position 34 bacterial lysate screen. (A) Bacterial lysate screen of RZnP0.41.3 mutants at position 34. (B) Dynamic range in HeLa cells of new mutants from the *in vitro* screen.

4.8 RZnP0.41.1 positions 33 and 34 mutagenesis

Because mutations in positions 33 and, particularly, 34 generated improved RZnP0.41.3 sensors, we went back and tested a few mutations in the same positions in RZnP0.41.1. After performing SDM at sights 33 and 34 separately, we obtained seven mutant sensors. Interestingly, one sensor appeared to have a stable response to Zn^{2+} + PTO, but the sensor was a turn-off Zn^{2+} sensor (Fig. 17A). Most other sensors tested showed a similar dynamic range compared to RZnP0.41.1 (Fig. 17B) and but all except RZnP0.41.1 H34L showed an unstable response to Zn^{2+} + PTO (Fig. 17C).

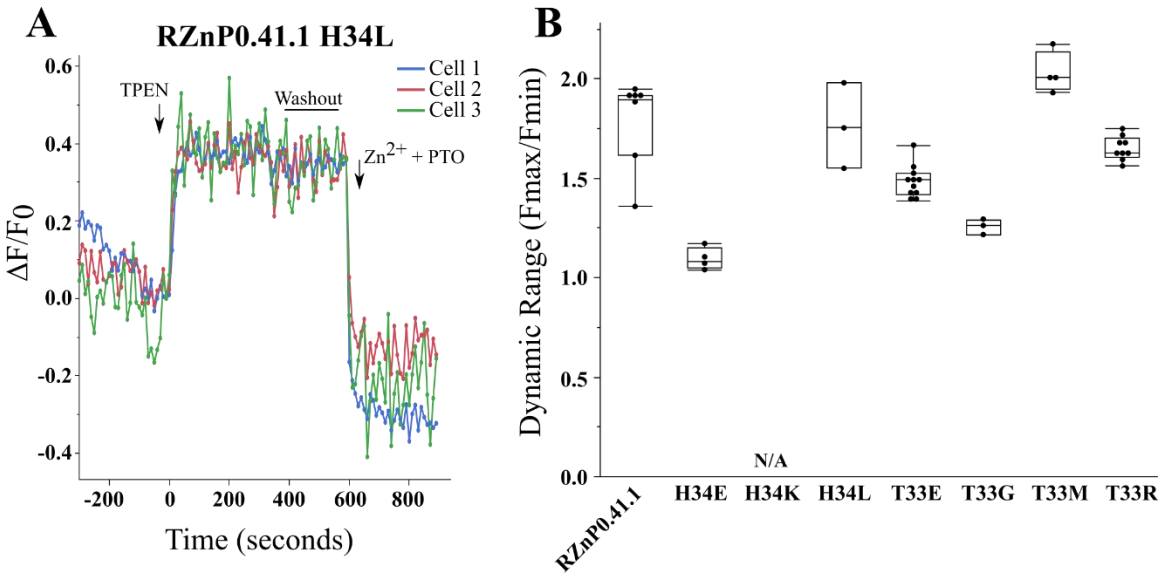

C

RZnP0.41.1 Mutants	*Increased Stability?*
RZnP0.41.1	-
H34E	No
H34K	No
H34L	Yes
T33E	No
T33G	No
T33M	No
T33R	No

Figure 17. RZnP0.41.1 positions 33 and 34 mutagenesis. In HeLa cells: (A) Zn^{2+} response curve of RZnP0.41.1 H34L. (B) Dynamic range of RZnP0.41.1 mutants. (C) Table indicating if any sensors had a stable response to Zn^{2+} + PTO.

5.0 DISCUSSION

5.1 Overall conclusions

In this work, RZnP1 (Fig. 8) was successfully developed. It was found that using the linker two region from R-GECO1 and mutating position 34 resulted in a RZnP1 that has a high dynamic range, ~4.3 fold, and high baseline fluorescence. Although the dynamic range is lower compared to the work done by Chen and Ai, the kinetics of the sensor are on the order of seconds, not minutes. This allows for resolution of quick movements of labile Zn^{2+} in the cell.

An advantage to having a RZnP, with the use of GZnP, is the ability to visualize labile Zn^{2+} in two different cellular compartents simultaneously, or a cellular compartment and the cytoplasm. Our RZnP1, based on the Zn^{2+} response curve, is believed to be a low affinity sensor. This is most likely due to mutating histidine, an amino acid Zn^{2+} can bind to, at posititon 34 to alanine. A similar decrease in affinity is seen between GZnP2 and GZnP3 when the histidine at position 34 is mutated.

This work also paves the way for using GZnPs in the ER. Using $0Ca^{2+}$ HHBSS buffer, we were able to get similar kinetics of our GZnP-ER sensors compared with our cytoplasmic GZnP sensors. We also obtained preliminary data that suggests the ER has lower labile Zn^{2+} concentration compare to the cytoplasm. However, the issue of a decreased dynamic range was never solved.

5.2 RZnP0.41.3 position 34 mutagenesis

What is interesting about mutating position 34 in RZnP0.41.3 is that all seven amino acids tested show an increased baseline fluorescence and a dynamic range around 4 fold. This indicates that, at least in the case of RZnP0.41.3, that histidine may be one of the worst amino acids in this location when trying to make a biologically relevant RZnP. Testing the other 12 amino acids that have not be observed *in situ* may reveal in even better RZnP. It is also likely that, because all other mutants in this position have comparable baseline fluorescence and dynamic ranges, that mutating this position may result in sensors that have no improvement over RZnP1.

5.3 GZnP-ER

The environment of the ER is much different than the cytoplasm. Identfying what component of the ER is changing our sensors is a difficult task. What is also difficult is trying to identify if the affinity for Zn^{2+} of our GZnP-ER sensors have changed. We currently do not have any method to test affinity of our sensors in the ER. We see that the reduction of the ER does not appear to affect dynamic range and the addition of additional residues on GZnP3, in the case of the GZnP3-KAAL mutant, does not affect its function in the cyptoplasm, so it does not appear that either of these two factors play a role in the defects of GZnP-ER sensors.

Agreeing with the discovery that additonal residues do not affect sensor function, the GZnP-KKYN plasmid can be a very useful proof of concenpt for localizing GZnPs to other locations in the secretory pathway without affecting sensor function beyond the

change in the environment from the cytoplasm. For example, sialyltransferase can be used to localize GZnPs to the trans-Golgi networkwhich has been shown to contain Zn^{2+}.

In addition to the challenges mentioned above, we are concerned about pH changes affecting the brightness of our sensor. We have developed an ER-pHuji, a fluorescent protein that detects pH changes localized to the ER, but this sensor has yet to be tested. In figure 14A-C and 16A we see TPEN increase the brightness of the sensors, which may be due to a known increase in pH upon additon of TPEN. This indicates that the GZnP-ER sensors are susceptible to pH just like any other FP sensor. Future work with these sensors should begin by identfying if any pH changes in the ER are affecting brightness of these sensors.

5.4 RZnP0.81 and a high affinity RZnP

The only mutations tested in RZnP0.81 that resulted in consistent functional sensors was in position 33. We found this position, at least in RZnP0.81, to be important for putatively increasing the affinity of the sensor for Zn^{2+}. When trying to retain the high affinity of RZnP0.81 Y33C and increasing dynamic range by mutating position 34, a position known to decrease affinity if a histidine is not in that location but also potentially increase dynamic range, we found no high affinity RZnPs with a high dynamic range. This was only done *in vitro* with a sensor that has a low baseline fluorescence and a dynamic range of ~1.47 fold; which may be unstable when responding to Zn^{2+}. It may be worth testing mutants in this position *in situ* to eliminate any potential error from the bacterial screen.

We attempted to use the information that a cysteine at position 33 may be involved in increasing affinity for Zn^{2+} to create a high affinity RZnP using RZnP1 as the parent sensor. Using this sensor, we mutated position 33 from a threonine to a cysteine. When tested in HeLa cells, we found that this sensor had reduced brightness, reduced dynamic range, is not stable when Zn^{2+} is added, and does not appear to have a higher affinity than RZnP1.

In the GZnP sensors, the histidine in position 34 was found to be important for the high affinity GZnP1 sensor. However, our only current sensors with high dynamic range have position 34 mutated, potentially eliminating this residue when considering positions to mutate to create a high affinity RZnP, at least in the case of RZnP0.41.3. Mutations of RZnP1 between residues 35-39 should be considered. These positions have been shown to affect sensor function but have yet to be mutated in our most optimized sensor. Mutations that increase affinity in the Zn^{2+} binding domains of ZF1 and ZF2 should also be explored.

5.5 Increased Stability of RZnP0.41

Originally, it was found that mutating position 36 of RZnP0.41 from serine to valine (RZnP0.41.1) increased the stability of the sensor when it was saturated with Zn^{2+}, although the sensor remained unstable. This changed the residue from a polar residue to a nonpolar residue that has the second smallest side chain of any amino acid. The only comparable mutants tested in this position are leucine and isoleucine. Both these amino acids have an additional CH_2 on their side chain and both residues are nonpolar. Even

being very similar to alanine, both these residues resulted in an unstable RZnP with a lower dynamic range and a similar unstable response to Zn^{2+} compared to RZnP0.41.

Moreover, mutating linker 1 to TR in RZnP0.41.1 resulted in a highly unstable and weak sensor. It was found again that position 36 is important in increasing the stability of the RZnP0.41 sensors as it was a mutation from valine to arginine that produced RZnP0.41.3, the parent sensor that was used to create RZnP1.

Only three mutated residues were tested in position 36 of RZnP0.41.2: arginine, lysine, and leucine. Interestingly, although arginine and lysine are very similar amino acids, the lysine mutation resulted in a worse sensor than RZnP0.41.2 while arginine produced RZnP0.41.3. Why similar amino acids have very different effects on the functionality of the sensor is hard to determine with our current screens, other methods such as analyzing the crystal structure of our sensors in apo- and saturated conditions of Zn^{2+} would need to be done to determine the interactions of these residues in the sensor on the atomic level (Shen et al. 2018a).

5.6 Future Directions

Beyond looking at baseline fluorescence and dynamic range of our new RZnPs, more detailed analysis of the properties of these sensors needs to be determined. The K_d of the new RZnPs is still unknown, we have no accurate kinetic analysis for the sensors, the pH stability has not been assessed, and analyzing the quantum yield and extinction coefficient will give use the best determination of "brightness" of the sensor. Affinity for Zn^{2+}, kinetics, and pH stability can all be determined by cloning the new RZnPs into a

pDisplay plasmid, which localizes the sensors to the extracellular matrix. This is advantageous for determining K_d because the sensors will not be competing with endogenous proteins when binding Zn^{2+}. It also allows us to see rapid increases in fluorescence upon Zn^{2+} saturation as we are not relying on PTO to shuttle Zn^{2+} into the cell, which relies on diffusion. And we can directly test pH sensitivity by adding different pH buffers to the imaging solution.

Although the current GZnP-ERs have been successfully targeted to the ER, currently have an unexplained reduced dynamic range. Along with this, there are concerns that changes in pH can drastically alter the brightness of these sensors. Further pH stability tests and hypothesis of why the dynamic range is reduced needs to be tested.

Despite the current set-backs, GZnPs were for the first time localized to the ER and displayed some functionality, and red fluorescent Zn^{2+} probes are now available to be used in the research of Zn^{2+} homeostasis.

References

Akerboom, J., T.-W. Chen, T. J. Wardill, L. Tian, J. S. Marvin, S. Mutlu, N. C. Calderón, F. Esposti, B. G. Borghuis, X. R. Sun, A. Gordus, M. B. Orger, R. Portugues, F. Engert, J. J. Macklin, A. Filosa, A. Aggarwal, R. A. Kerr, R. Takagi, S. Kracun, E. Shigetomi, B. S. Khakh, H. Baier, L. Lagnado, S. S. H. Wang, C. I. Bargmann, B. E. Kimmel, V. Jayaraman, K. Svoboda, D. S. Kim, E. R. Schreiter & L. L. Looger (2012) Optimization of a GCaMP Calcium Indicator for Neural Activity Imaging. *The Journal of Neuroscience,* 32**,** 13819.

Andreini, C., L. Banci, I. Bertini & A. Rosato (2006) Counting the zinc-proteins encoded in the human genome. *J Proteome Res,* 5**,** 196-201.

Aronson, D. E., L. M. Costantini & E. L. Snapp (2011) Superfolder GFP is fluorescent in oxidizing environments when targeted via the Sec translocon. *Traffic,* 12**,** 543-8.

Botman, D., D. H. de Groot, P. Schmidt, J. Goedhart & B. Teusink (2019) In vivo characterisation of fluorescent proteins in budding yeast. *Scientific Reports,* 9**,** 2234.

Burdette, S. C., G. K. Walkup, B. Spingler, R. Y. Tsien & S. J. Lippard (2001) Fluorescent Sensors for Zn2+ Based on a Fluorescein Platform: Synthesis, Properties and Intracellular Distribution. *Journal of the American Chemical Society,* 123**,** 7831-7841.

Chabosseau, P., E. Tuncay, G. Meur, E. A. Bellomo, A. Hessels, S. Hughes, P. R. Johnson, M. Bugliani, P. Marchetti, B. Turan, A. R. Lyon, M. Merkx & G. A. Rutter (2014) Mitochondrial and ER-targeted eCALWY probes reveal high levels of free Zn2+. *ACS Chem Biol,* 9**,** 2111-20.

Chasapis, C. T., P.-S. A. Ntoupa, C. A. Spiliopoulou & M. E. Stefanidou (2020) Recent aspects of the effects of zinc on human health. *Archives of Toxicology,* 94**,** 1443-1460.

Chen, Z. & H. W. Ai (2016) Single Fluorescent Protein-Based Indicators for Zinc Ion (Zn(2+)). *Anal Chem,* 88**,** 9029-36.

Crevenna, A. H., B. Blank, A. Maiser, D. Emin, J. Prescher, G. Beck, C. Kienzle, K. Bartnik, B. Habermann, M. Pakdel, H. Leonhardt, D. C. Lamb & J. von Blume (2016) Secretory cargo sorting by Ca2+-dependent Cab45 oligomerization at the trans-Golgi network. *J Cell Biol,* 213**,** 305-14.

Dana, H., B. Mohar, Y. Sun, S. Narayan, A. Gordus, J. P. Hasseman, G. Tsegaye, G. T. Holt, A. Hu, D. Walpita, R. Patel, J. J. Macklin, C. I. Bargmann, M. B. Ahrens, E. R. Schreiter, V. Jayaraman, L. L. Looger, K. Svoboda & D. S. Kim (2016) Sensitive red protein calcium indicators for imaging neural activity. *Elife,* 5.

Dean, K. M., Y. Qin & A. E. Palmer (2012) Visualizing metal ions in cells: An overview of analytical techniques, approaches, and probes. *Biochimica et Biophysica Acta (BBA) - Molecular Cell Research,* 1823**,** 1406-1415.

Dittmer, P. J., J. G. Miranda, J. A. Gorski & A. E. Palmer (2009) Genetically encoded sensors to elucidate spatial distribution of cellular zinc. *J Biol Chem,* 284**,** 16289-16297.

Fudge, D. H., R. Black, L. Son, K. LeJeune & Y. Qin (2018) Optical Recording of Zn(2+) Dynamics in the Mitochondrial Matrix and Intermembrane Space with the GZnP2 Sensor. *ACS Chem Biol,* 13**,** 1897-1905.

Gandasi, N. R., K. Vestö, M. Helou, P. Yin, J. Saras & S. Barg (2015) Survey of Red Fluorescence Proteins as Markers for Secretory Granule Exocytosis. *PLoS One,* 10**,** e0127801.

Gee, K. R., Z. L. Zhou, D. Ton-That, S. L. Sensi & J. H. Weiss (2002) Measuring zinc in living cells.: A new generation of sensitive and selective fluorescent probes. *Cell Calcium,* 31**,** 245-251.

Kambe, T., T. Tsuji, A. Hashimoto & N. Itsumura (2015) The Physiological, Biochemical, and Molecular Roles of Zinc Transporters in Zinc Homeostasis and Metabolism. *Physiological Reviews,* 95**,** 749-784.

Krezel, A. & W. Maret (2006) Zinc-buffering capacity of a eukaryotic cell at physiological pZn. *J Biol Inorg Chem,* 11**,** 1049-62.

Mahanand, D. & J. C. Houck (1968) Fluorometric Determination of Zinc in Biologic Fluids. *Clinical Chemistry,* 14**,** 6-11.

Minckley, T. F., C. Zhang, D. H. Fudge, A. M. Dischler, K. D. LeJeune, H. Xu & Y. Qin (2019) Sub-nanomolar sensitive GZnP3 reveals TRPML1-mediated neuronal Zn(2+) signals. *Nat Commun,* 10**,** 4806.

Miranda, J. G., A. L. Weaver, Y. Qin, J. G. Park, C. I. Stoddard, M. Z. Lin & A. E. Palmer (2012) New alternately colored FRET sensors for simultaneous monitoring of Zn^{2+} in multiple cellular locations. *PLoS One,* 7**,** e49371.

Nagai, T., A. Sawano, E. S. Park & A. Miyawaki (2001) Circularly permuted green fluorescent proteins engineered to sense Ca<sup>2+</sup&gt. *Proceedings of the National Academy of Sciences,* 98**,** 3197.

Qiao, W., M. Mooney, A. J. Bird, D. R. Winge & D. J. Eide (2006) Zinc binding to a regulatory zinc-sensing domain monitored in vivo by using FRET. *Proc Natl Acad Sci U S A,* 103**,** 8674-9.

Qin, Y., P. J. Dittmer, J. G. Park, K. B. Jansen & A. E. Palmer (2011) Measuring steady-state and dynamic endoplasmic reticulum and Golgi Zn2+ with genetically encoded sensors. *Proc Natl Acad Sci U S A,* 108**,** 7351-6.

Qin, Y., J. G. Miranda, C. I. Stoddard, K. M. Dean, D. F. Galati & A. E. Palmer (2013) Direct Comparison of a Genetically Encoded Sensor and Small Molecule Indicator: Implications for Quantification of Cytosolic Zn2+. *ACS Chemical Biology,* 8**,** 2366-2371.

Qin, Y., D. W. Sammond, E. Braselmann, M. C. Carpenter & A. E. Palmer (2016) Development of an Optical Zn(2+) Probe Based on a Single Fluorescent Protein. *ACS Chem Biol,* 11**,** 2744-2751.

Rivera-Fuentes, P., A. T. Wrobel, M. L. Zastrow, M. Khan, J. Georgiou, T. T. Luyben, J. C. Roder, K. Okamoto & S. J. Lippard (2015) A far-red emitting probe for unambiguous detection of mobile zinc in acidic vesicles and deep tissue. *Chemical Science,* 6**,** 1944-1948.

Samtleben, S., J. Jaepel, C. Fecher, T. Andreska, M. Rehberg & R. Blum (2013) Direct imaging of ER calcium with targeted-esterase induced dye loading (TED). *J Vis Exp***,** e50317.

Shen, Y., H. Dana, A. S. Abdelfattah, R. Patel, J. Shea, R. S. Molina, B. Rawal, V. Rancic, Y.-F. Chang, L. Wu, Y. Chen, Y. Qian, M. D. Wiens, N. Hambleton, K. Ballanyi, T. E. Hughes, M. Drobizhev, D. S. Kim, M. Koyama, E. R. Schreiter & R. E. Campbell (2018a) A genetically encoded Ca2+ indicator based on circularly permutated sea anemone red fluorescent protein eqFP578. *BMC Biology,* 16**,** 9.

Shen, Y., H. Dana, A. S. Abdelfattah, R. Patel, J. Shea, R. S. Molina, B. Rawal, V. Rancic, Y. F. Chang, L. Wu, Y. Chen, Y. Qian, M. D. Wiens, N. Hambleton, K. Ballanyi, T. E. Hughes, M. Drobizhev, D. S. Kim, M. Koyama, E. R. Schreiter & R. E. Campbell (2018b) A genetically encoded Ca(2+) indicator based on circularly permutated sea anemone red fluorescent protein eqFP578. *BMC Biol,* 16**,** 9.

Stork, C. J. & Y. V. Li (2006) Intracellular Zinc Elevation Measured with a "Calcium-Specific" Indicator during Ischemia and Reperfusion in Rat Hippocampus: A Question on Calcium Overload. *The Journal of Neuroscience,* 26**,** 10430-10437.

Tian, L., S. A. Hires, T. Mao, D. Huber, M. E. Chiappe, S. H. Chalasani, L. Petreanu, J. Akerboom, S. A. McKinney, E. R. Schreiter, C. I. Bargmann, V. Jayaraman, K. Svoboda & L. L. Looger (2009) Imaging neural activity in worms, flies and mice with improved GCaMP calcium indicators. *Nat Methods,* 6**,** 875-81.

van Dongen, E. M. W. M., L. M. Dekkers, K. Spijker, E. W. Meijer, L. W. J. Klomp & M. Merkx (2006) Ratiometric Fluorescent Sensor Proteins with Subnanomolar Affinity for Zn(II) Based on Copper Chaperone Domains. *Journal of the American Chemical Society,* 128**,** 10754-10762.

van Dongen, E. M. W. M., T. H. Evers, L. M. Dekkers, E. W. Meijer, L. W. J. Klomp & M. Merkx (2007) Variation of Linker Length in Ratiometric Fluorescent Sensor Proteins Allows Rational Tuning of Zn(II) Affinity in the Picomolar to Femtomolar Range. *Journal of the American Chemical Society,* 129**,** 3494-3495.

Vinkenborg, J. L., T. J. Nicolson, E. A. Bellomo, M. S. Koay, G. A. Rutter & M. Merkx (2009) Genetically encoded FRET sensors to monitor intracellular Zn2+ homeostasis. *Nat Methods,* 6**,** 737-40.

Zerangue, N., M. J. Malan, S. R. Fried, P. F. Dazin, Y. N. Jan, L. Y. Jan & B. Schwappach (2001) Analysis of endoplasmic reticulum trafficking signals by combinatorial screening in mammalian cells. *Proceedings of the National Academy of Sciences,* 98**,** 2431-2436.

Zhao, Y., S. Araki, J. Wu, T. Teramoto, Y. F. Chang, M. Nakano, A. S. Abdelfattah, M. Fujiwara, T. Ishihara, T. Nagai & R. E. Campbell (2011) An expanded palette of genetically encoded Ca^{2+} indicators. *Science,* 333**,** 1888-91.

Appendix A

Abbreviations:

Calcium: Ca^{2+}
Cartilage oligomeric matrix protein: COMP
Circularly permutated fluorescent protein: cpFP
Endoplasmic reticulum: ER
Förster resonance energy transfer: FRET
Green fluorescent protein: GFP
Green zinc probe: GZnP
Magnesium: Mg^{2+}
Monomeric teal fluorescent protein: mTFP1
N,N,N′,N′-tetrakis(2-pyridinylmethyl)-1,2-ethanediamine: TPEN
Pyrithione: PTO
Red fluorescent protein: RFP
Red zinc probe: RZnP
Signal sequence: SS
Site directed mutagenesis: SDM
Zinc: Zn^{2+}
Zinc finger: ZF